Materials Science & Engineering C 131 (2021) 112516

Contents lists available at ScienceDirect

Materials Science & Engineering C

journal homepage: www.elsevier.com/locate/msec

Extracellular matrix-inspired surface coatings functionalized with dexamethasone-loaded liposomes to induce osteo- and chondrogenic differentiation of multipotent stem cells

Yazmin A. Brito Barrera [a], Catharina Husteden [b], Jumanah Alherz [a], Bodo Fuhrmann [c], Christian Wölk [d], Thomas Groth [a,c,e,*]

[a] Department Biomedical Materials, Institute of Pharmacy, Martin Luther University Halle–Wittenberg, Heinrich-Damerow-Strasse 4, 06120 Halle (Saale), Germany
[b] Medicinal Chemistry Department, Institute of Pharmacy, Martin Luther University Halle-Wittenberg, 06120 Halle (Saale), Germany
[c] Interdisciplinary Center of Materials Science, Martin Luther University Halle-Wittenberg, D-06099 Halle (Saale), Germany
[d] Pharmaceutical Technology, Institute of Pharmacy, Faculty of Medicine, Leipzig University, 04317 Leipzig, Germany
[e] Laboratory of Biomedical Nanotechnologies, Institute of Bionic Technologies and Engineering, I.M. Sechenov First Moscow State University, 119991, Trubetskaya street 8, Moscow, Russian Federation

ARTICLE INFO

Keywords:
C3H10T1/2 cells
Cationic lipids
Hyaluronic acid
Collagen I
Dexamethasone
Osteogenic/chondrogenic differentiation
Polyelectrolyte multilayer system

ABSTRACT

Biomimetic surface coatings can be combined with conventional implants to mimic the extracellular matrix (ECM) of the surrounding tissue to make them more biocompatible. Layer-by-layer technique (LbL) can be used for making surface coatings by alternating adsorption of polyanions and polycations from aqueous solutions without need of chemical reactions. Here, polyelectrolyte multilayer (PEM) systems is made of hyaluronic acid (HA) as polyanion and Collagen I (Col) as polycation to mimic the ECM of connective tissue. The PEM are combined with dexamethasone (Dex)-loaded liposomes to achieve a local delivery and protection of this drug for stimulation of osteo- and chondrogenic differentiation of multipotent stem cells. The liposomes possess a positive surface charge that is required for immobilization on the PEM. The surface properties of PEM system show a positive zeta potential after liposome adsorption and a decrease in wettability, both promoting cell adhesion and spreading of C3H10T1/2 multipotent embryonic mouse fibroblasts. Differentiation of C3H10T1/2 was more prominent on the PEM system with embedded Dex-loaded liposomes compared to the basal PEM system and the use of free Dex-loaded liposomes in the supernatant. This was evident by immunohistochemical staining and an upregulation of the expression of genes, which play a key role in osteogenesis (RunX2, ALP, Osteocalcin (OCN)) and chondrogenesis (Sox9, aggrecan (ACAN), collagen type II), determined by quantitative Real-time polymerase chain reaction (qRT-PCR) after 21 days. These findings indicate that the designed liposome-loaded PEM system have high potential for use as drug delivery systems for implant coatings that can induce bone and cartilage differentiation needed for example in osteochondral implants.

Abbreviations: ALP, Alkaline Phosphatase; ACAN, aggrecan; AFM, Atomic force microscopy; ASC, ascorbic acid; BMP, bone morphogenetic proteins; CLSM, Confocal Laser Scanning Microscopy; Col, Collagen I; Dex, Dexamethasone; DMEM, Dulbecco's modified Eagle's medium; DOPE, dioleoylphosphatidylethanolamine; ECM, Extracellular matrix; FCS, Fetal calf serum; GAG, Glycosaminoglycan; ß-Gly, β-Glycerophosphate; HA, Hyaluronic acid; RHAMM, hyaluronan-mediated motility; LbL, Layer-by-Layer; (MKP-1), Mitogen-activated protein kinase phosphatase 1; PBS, Phosphate-buffered saline; PEI, Polyethylenimine; PEM, polyelectrolyte multilayer system; qRT-PCR, Quantitative Real-time polymerase chain reaction; OO4, *N*-{6-amino-1-[*N*-(9*Z*)-octadec-9-enylamino]-1-oxohexan-(2*S*)-2-yl}-*N'*-{2-[*N*,*N*-bis(2-aminoethyl)amino] ethyl}-2-hexadecylpropandiamide; OCD, osteochondral defect; OCN, Osteocalcin; SN, supernatant; SPR, Surface plasmon resonance; TAZ, (transcriptional co-activator with PDZ-binding motif); WCA, Water contact angle.

* Corresponding author at: Department Biomedical Materials, Institute of Pharmacy, Martin-Luther-University Halle-Wittenberg, Heinrich-Damerow-Strasse 4, 06120 Halle (Saale), Germany.
E-mail address: thomas.groth@pharmazie.uni-halle.de (T. Groth).

https://doi.org/10.1016/j.msec.2021.112516
Received 27 August 2021; Received in revised form 19 October 2021; Accepted 22 October 2021
Available online 29 October 2021

1. Introduction

Bone and cartilages defects are common disorders affecting people of all ages. These defects are caused by trauma, tumors, infections, and congenital diseases [1,2]. One example are osteochondral defects (OCD) that affect both articular cartilage and subchondral bone as important components of joints in the body [2,3]. The articular cartilage protects the subchondral bone from contact pressure and permits low friction movements of the joint [3]. Commonly, the cartilage and subchondral bone undergo degeneration as the result of osteoarthritis, which requires often surgical interventions [2]. The more recent management of OC lesions does not only aim to relieving patients from pain and repairing damaged tissue but also restoring functionality of the joint [4]. Conventional therapies include drilling techniques, abrasion, micro fracture as well as transplantation of OC allografts and autologous chondrocyte implantation [5,6]. Unfortunately, severe OC defects often require total joint replacement implanting artificial joints made of metals, ceramics and durable polymers [4]. However, these materials are not bioactive, which may cause delayed healing or induction of inflammation as undesired effects [4]. Therefore, coating the implant surface – particularly the metallic parts that are inserted in the bone - with materials that promote engrafting like bioactive calcium phosphates or polymers has been suggested [4].

One of the techniques for surface coating of implants is the Layer-by-Layer technique (LbL) [7]. This surface coating method was established by Decher and coworkers [8] and is based on cycles of alternating adsorption of polyanions and polycations from aqueous solutions onto charged surfaces [8]. LbL has been widely used for various biomedical applications including tissue engineering, medical implants, regenerative medicines, and drug delivery [9–12]. For instance, multilayers made of biogenic polyelectrolytes such as collagen and glycosaminoglycans have been found to guide cell adhesion and function because they mimic partly the composition of extracellular matrix (ECM) of connective tissue [13].

Surface coatings based on LbL can be used to improve biocompatibility of implants but also to deliver a drug locally [14]. A limitation of pharmaceutical treatment of OC defects is that the systemic delivery of drugs is not leading to the desired local effect and it may have systemic side effects [15]. Hence, the advantages of a local delivery are to bring the agent to the target, reducing the drug amount, toxicity and other harmful local and systemic side effects [16,17]. Options to deliver a drug with an orthopedic implant or scaffold can be based on coating the drug on the implant surface or blending the drug with the biomaterials during production [15]. Nowadays, bone regeneration after complicated fractures or larger bone defects is achieved by use of growth factors like bone morphogenetic proteins (BMP), transforming growth factors, and growth hormones [15] to promote cell adhesion, proliferation, and differentiation [18]. However, a limitation of the current clinical use of growth factors like BMP-2, is the high cost and dosage used because of their fast degradation. Particularly the high dosage of growth factors like BMP-2 in mg scale in some clinical applications can have negative local and systemic side effects [19,20]. Therefore, local delivery of small quantities in microgram scale as suggested by Salmeron-Sanchez and coworkers [20] may provide a better solution for regeneration of bone.

On the other hand, nano-sized materials can be applied as systems for release of bioactive agents that can be used in regenerative medicine and treatment of cancer. Liposomes are interesting since they can carry different types of drugs because of their aqueous inner compartment and the hydrophobic part of the lipid bilayer. For example, liposomes have been applied for the delivery of dexamethasone (Dex) to regenerate bone [5,21]. They can be also applied for transfection of cells by the delivery of nucleic acids [22], since positively charged liposomes and lipoplexes can be efficiently internalized into cells. We could show recently that liposomes composed of dioleylphosphatidylethanolamine (DOPE) and the ionizable lipid *N*-{6-amino-1[*N*-(9*Z*)-octadec-9-enylamino]-1-oxohexan-(2*S*)-2-yl}-*N*′-{2-[*N*,*N*-bis(2-aminoethyl)amino]ethyl}-2[(9*Z*)-octadec9enyl]propandiamide (OO4) represent an excellent carrier for drug delivery in cells [23–25]. Overall, liposomes possess a very wide spectrum of application as drug-delivery systems for charged molecules [26], of anti-microbial agents [27], as vaccine carriers [28], transfection agents [29], and delivery of growth and differentiation factors such as BMP-2, TGF, and Dex [21,30]. In addition, liposomes can be used as component for formation of multilayers by LbL due to their inherent charge, which permits localized delivery of drugs avoiding systemic effects [31].

Previous studies combining vesicular structures with polyelectrolytes to fabricate multilayers (PEM) were made using phosphatidylcholine (PC) liposomes, doped with phosphatidylserine (PS) or phosphatidylglycerol (PG) and stabilized with poly-L-lysine (PLL) into PEMs composed of synthetic polymers [32,33]. However, these studies were focussed predominantly on the material science aspects. There are also previous investigations using PC liposomes embedded in different PEM systems to study their interactions with cells. For example, Graf et al. described efficient encapsulation of calcein-loaded PS-containing liposomes into PEMs fabricated from synthetic polymers and their delivery into cells [34]. Demuth et al. described an PEM based systems with embedded liposomes to deliver antigens into the skin via deposition on microneedles [35]. Further approaches created backpacks for cells loaded with echogenic liposomes which encapsulate doxorubicin as potential cancer therapy [36]. A very recent work describes the embedding of liposomes in multilayers as model for exosomes by LbL but used a dye for the evidence of transfer into cells [37]. However so far, no studies reported about the combination of liposomes with LbL for controlled release to engineer connective tissue have been reported.

In tissue engineering, mesenchymal stem cells (MSC) have been used for several years due to their potential to differentiate into various tissues such as muscle, fat, bone, and cartilage and others [38]. C3H10T1/2 is a mesenchymal stem cell line that was obtained from a mouse embryo and can differentiate into various phenotypic lineages such as adipocytes, chondrocytes and osteoblasts by different inductive mediators [39,40]. The phenotypic features and differentiation of MSC to bone and cartilage cells include markers, such as alkaline phosphatase, deposition of calcium phosphate, and the expression of various ECM proteins such as collagen type I (Col) and II, osteocalcin (OCN), proteoglycans like aggrecan (ACAN), and glycosaminoglycans (GAG), etc. [41]. Moreover, it involves the detection of specific transcription factors, which are known to control mesenchymal cell differentiation towards chondrogenic or osteogenic lineages [41]. The transcription factors, Runx2, Osterix, and β-catenin, regulate osteoblast differentiation. Sox family transcription factors like Sox9 regulate chondrocyte differentiation [42]. Further, mesenchymal progenitors are initially marked by expression of Sox9, followed by Runx2 leading to the development of osteoblast [36]. However, cells with Sox9 expression are bipotential and can also differentiate into chondrocytes [42]. The addition of an inductive mediator like Dex can influence both osteogenic and chondrogenic differentiation. [19,38]. Dex can activate β-catenin mediated transcription and this activation induces Runx2 expression and upregulates TAZ and MKP1 that also promote Runx2 activity [43,44]. For chondrogenesis, Dex enhance the expression of Sox9 and activates the gene expression of type II procollagen (Col2a1) and ACAN [45].

OC defects require repair of bone and cartilage together, which means that implant materials or scaffolds should induce osteogenesis in the bone and chondrogenesis in the cartilage part of the defect. Hence, we were interested in elucidating the potential of Dex-loaded cationic liposomes to induce both osteo- and chondrogenic differentiation in C3H10T1/2 cells. Two approaches were combined to develop a functionalized surface coating: (i) an LbL surface coating that mimics the natural ECM of connective tissue by combination of Col and HA in PEM system and (ii) the immobilization of Dex-loaded liposomes for potential local delivery at the defect site. This research presents the physicochemical characteristics of the multilayer films, such as surface zeta potential, thickness, layer growth, and wettability. Cell studies with

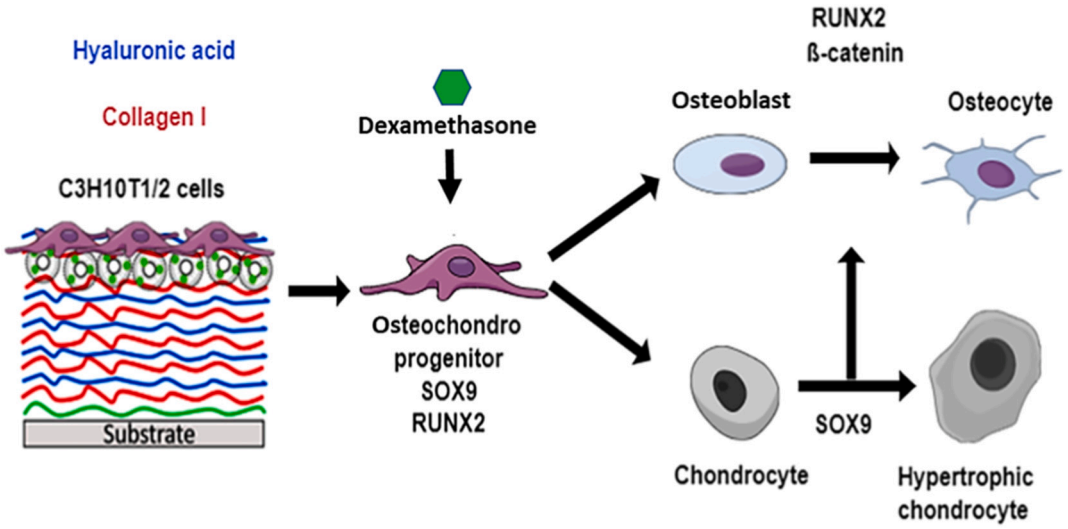

Fig. 1. Schematic illustration of the influence of the Dex in combination with polyelectrolyte multilayer in the regulation of osteoblast and chondrocyte differentiation by Sox9 and Runx2. During the process of osteoblast differentiation, Dex is an important compound for induction of mesenchymal stem cells to osteoblast lineage and clearly influences early stages of osteoblast differentiation as well as for chondrogenesis. Dex begins to play a key role in osteoblast differentiation by activating the Runx2-mediated and β-catenin pathways. For the period of chondrocyte differentiation initiated by Sox9-mediated mesenchymal condensation.

multipotent murine C3H10T1/2 cells evaluated the advantage of using liposomes loaded with Dex immobilized in PEMs to induce both osteogenic and chondrogenic differentiation (Fig. 1).

2. Materials and methods

2.1. Preparation of cationic liposomes

The lipid film hydration procedure was applied for the preparation of liposomes. Briefly, OO4 and DOPE lipids were separately dissolved in chloroform/methanol (8:2, *v*/v) to get stock solutions of 2 mg mL^{-1}. The stocks were mixed in the molar ratio 1:3 OO4/DOPE (M OO4 = 860.39 g mol^{-1}, M DOPE = 744.03 g mol^{-1}). The solvent was evaporated, and the obtained thin lipid film was dissolved in water containing 0.15 M of sodium chloride (Carl Roth GmbH, Karlsruhe, Germany) and (0.1 M, final pH 4) acetic acid (Carl Roth GmbH, Karlsruhe, Germany) to obtain a lipid concentration of 1 mg·mL^{-1}. For the film hydration at 50 °C at 1400 rpm, an Eppendorf Thermomixer 5436 was used for 30 min followed by sonication using a bath sonicator at 37 kHz, 6 cycles for 3 min, while the last cycle was at 70 °C for 4 min. The liposomes were prepared in batch sizes of 1 to 10 mL.

2.1.1. Loading of cationic liposomes with dexamethasone

The liposomes were prepared with a concentration of 1 mg mL^{-1} total lipid (50 μg mL^{-1} Dex) following the liposome preparation protocol explained in previous studies [46] using chloroform/methanol (8:2, *v*/v) stock solutions of OO4, DOPE and Dex combined to a molar ratio of 1:3:0.2 (n_{OO4}:n_{DOPE}:n_{Dex}).

2.1.2. Characterization of liposomes

The size of liposomes was determined by dynamic light scattering (DLS) and zeta potential by laser Doppler velocimetry (lDv) using a Zetasizer Nano ZS ZEN3600 (Malvern Panalytical). DLS measurements were performed in half-volume cuvettes in three independent measurements consisting of 15 runs with a duration time of 20 s for each run at 25 °C. The scattering angle was 173°. For the calculations, a viscosity η = 0.8872 mPa s and a refractive index of 1.33 were assumed and the autocorrelation function was evaluated by Zetasizer Software 7.13 (Malvern Panalytical). lDv was performed in a clear disposable folded capillary cell (DTS1060, Malvern Panalytical). Three independent measurements involving 30 runs with a voltage of 60 V were performed at 25 °C. For the calculations, the viscosity (η = 0.8872 mPa s), dielectric constant (ε = 78.5 F m^{-1}) and refractive index (*n* = 1.33) of water were assumed. The mobility μ of the diffusing aggregates was converted into the ζ potential using the Smoluchowski relationship ζ = μ η/ε (Zetasizer Software 7.13).

2.2. Preparation of substrata

Before the deposition of polyelectrolyte multilayers on glass coverslips (ø 12 mm, VWR, Germany) and silicon wafers (Silicon materials, Kaufering, Germany), organic residues were eliminated after the RCA-1 method. This method suggests mixing the following solutions: ultra-pure water, ammonium hydroxide (Carl Roth GmbH, Karlsruhe, Germany), and hydrogen peroxide (Carl Roth GmbH, Karlsruhe, Germany) in the ratio of 5:1:1, respectively. The gold-coated glass sensor for surface plasmon resonance (SPR, IBIS Technologies BV, Enschede, Netherlands. 10 × 10 mm^2) were treated by dipping into 0.5 M NaOH in 96% ethanol and followed by rinsing with ethanol (99%) and one last rinsing step with micro pure water followed by drying with nitrogen.

2.3. Glycosaminoglycan and collagen I solution preparation

The first solution required in the polyelectrolyte multilayer system was polyethylenimine (PEI). PEI (Mw ~ 750 kDa) provided from Sigma-Aldrich (Steinheim, Germany) was dissolved in 0.15 M sodium chloride (Carl Roth GmbH, Karlsruhe, Germany) solution at a concentration of 2 mg·mL^{-1}. A solution of sodium hyaluronate (HA) was used as a negatively charged polyelectrolyte for the multilayer assembly. Therefore, hyaluronic acid sodium salt (Mw ~ 1.2 MDa) Kraeber & Co GmbH (Ellerbeck, Germany) was dissolved in 0.15 M sodium chloride solution at a concentration of 0.5 mg mL^{-1}. The positively charged Col was used as third solution. Col from porcine skin (Mw ~ 100 kDa) was provided by Sichuan Mingrang Bio-Tech (Sichuan, China) and was dissolved in 0.2 M acetic acid (Carl Roth GmbH, Karlsruhe, Germany) in a concentration of 2 mg·mL^{-1} as a stock solution and stored in a temperature of 4 °C. Then, it was diluted with sodium chloride solution (0.15 M) to obtain a final concentration of 0.5 mg·mL^{-1}. The pH value of all solutions was adjusted to pH 4.

2.4. Preparation of polyelectrolyte multilayers

PEM were fabricated on cleaned glass coverslips, gold sensor, and silicon substrates, respectively, depending on the method used afterwards. PEM were fabricated in 24 well plates with 500 μL volume of each solution. PEI was applied as the initial layer by incubation of 15 min to get a positively charged surface. The first layer was formed by the application of polyanion solution (HA solution) for 15 min. The second layer was the polycation solution (Col solution) incubated for 20 min. Each deposition step was followed by washing with 0.15 M sodium chloride for five minutes, trice. The application of HA and Col solutions alternated until the ninth layer for liposomes was added. Twelve layers were used for unloaded PEM system $[HA/Col]_6$ in experiments with liposome-free PEMs. For LbL coatings with embedded liposomes, PEMs with the sequence $[HA/Col]_4$ were built like described above, followed by a HA layer to get the negative surface for adsorption of the positively charged Dex-loaded liposomes. For liposome deposition, the incubation time was 150 min. This layer was followed by deposition of an additional HA and Col layer to reach the final sequence [HA/Col]4HA/Lip [HA/Col].

2.5. Characterization of polyelectrolyte multilayers and surface properties

2.5.1. Ellipsometry

The PEM systems were prepared on silicon wafers. The thickness of PEMs was estimated by the use of ellipsometry (M-2000 V scanning ellipsometer, J.A. Woollam Co. Inc., Lincoln, NE, USA) at room temperature. The measurements were taken at incident angles of 60, 65, 70, and 75 of linear polarized light to the normal surface. The data were analyzed using the software WVase32.

2.5.2. Surface plasmon resonance

The measurements were conducted with an IBIS-iSPR device (IBIS Technologies BV, Enschede, Netherlands). The gold sensor was coated with 11-mercaptoundecanoic acid (MUDA) (Steinheim, Germany), mounted in a flow chamber, and equilibrated with sodium chloride to obtain a stable baseline. Then, the polyelectrolyte solution was injected at a flow rate of 3 μL s^{-1} followed by rinsing with sodium chloride for 15 min. PEI was added for 15 min, HA for 15 min, Col for 20 min and liposomes solution for 150 min until 13 layers were formed. The average of the shift values (m°) of each rinsing step was used for plotting the graphs and removing any unbound molecules.

2.5.3. ζ-Potential measurements

SurPASS electrokinetic (Anton Paar, Graz, Austria) was used to estimate the zeta-potential of PEM-coated glass substrates (10 × 20 mm2). The samples were mounted on the gap cell with double-sided tape. The used model electrolyte was 1 mmol·L-1 KCl in water (Carl Roth GmbH, Karlsruhe, Germany) solution. The pH titration solution from pH 3.0 to 10 (acid-based pH) was 0.1 mol·L-1 sodium hydroxide (Carl Roth GmbH, Karlsruhe, Germany). The analyzer was adjusted during the measurement process to a flow rate of 100–150 mL·min-1 at a maximum pressure of 300 mbar.

2.5.4. Water contact angle measurements

The wettability of the PEM was measured by static WCA using an OCA15+ device from Dataphysics (Filderstadt, Germany). The PEMs were prepared using glass cover slips. The sessile drop method was applied using 1 μL of water with the Ellipse-fitting method. The experiments were run in duplicates with five droplets per sample. Means and standard deviations were calculated.

2.5.5. Fluorescence microscopy of PEMs

PEMs were prepared according to the description in Section 2.4 using FITC-labeled HA and Rhodamine-DOPE labeled OO4/DOPE liposomes. The FITC-labelling of HA was done according to protocol published [47]. The micrographs were taken with confocal laser scanning microscopy (CLSM 701, Carl Zeiss Micro-Imaging GmbH, Jena, Germany) using a 63× oil immersion objective. Images were processed with the ZEN2012 software (Carl Zeiss).

2.6. Cell culture conditions

Cryopreserved C3H10T1/2 murine cell line (ATCC; LGC Promochem, Molsheim, France) were thawed and grown in DMEM low glucose medium supplemented with 10% heat-inactivated fetal calf serum and 1% antibiotic solution (penicillin/streptomycin) solution all provided by Biochrom AG (Berlin, Germany). Cultured cells were grown at 37 °C in a humidified 5% CO_2/95% air atmosphere using a NUAIRE DH Autoflow incubator (NuAire Corp., Plymouth, Minnesota, USA). Cells of almost confluent cultures were washed once with sterile PBS, followed by treatment with 0.25% trypsin/0.02% EDTA (Biochrom) at 37 °C for 3 min. Trypsin was neutralized with DMEM with 10% FCS, and cells were re-suspended in DMEM after centrifugation at 250*g* for 5 min. Finally, the cells were seeded on PEM coated glass coverslips at different concentrations depending on the assay.

2.7. Cell adhesion and growth

2.7.1. Cell adhesion studies

C3H10T1/2 cells were seeded on glass coverslips coated with PEM that were placed into 24 well plates at a density of 20.000 cell·mL^{-1} in DMEM supplemented with 10% FCS. After incubation at 37 °C for 4 h, cells attached to PEM were fixed with 4% paraformaldehyde solution (RotiHistofix, Carl Roth GmbH, Karlsruhe, Germany) for 10 min. After rinsing with PBS twice, the cells were permeabilized with 0.1% Triton X-100 in PBS (*v*/v) Sigma-Aldrich Chemie GmbH (Taufkirchen, Germany) for 10 min. After rinsing with PBS, nonspecific binding sites were blocked by incubation with 1% (*w/v*) bovine serum albumin (BSA, Merck, Darmstadt, Germany) in PBS at room temperature for 1 h. The vinculin was stained using primary mouse antibody (1:100, Sigma) and secondary Cy2- conjugated goat anti-mouse antibody (1:100, Dianova). Actin cytoskeleton was visualized by incubating the samples with Phalloidin CruzFluor 555 (1:1000, Santa Cruz Biotechnology, Heidelberg, Germany) at room temperature for 30 min. Cell nuclei were visualized by TO-PRO3 staining (1:500, Invitrogen, Darmstadt, Germany) incubating for 30 min. The samples were washed with PBS and mounted with Roti-Mount FluorCare (Carl Roth GmbH, Karlsruhe, Germany) and examined with confocal laser scanning microscopy (CLSM 701, Carl Zeiss Micro-Imaging GmbH, Jena, Germany) using 10× objective for cell counting, 20× objective for measurements of cell area and 63× oil immersion objective for visualization of focal adhesions, actin and nuclei. Images were processed with the ZEN2012 software (Carl Zeiss). The image analysis, such as cell count and cell area was performed with Image J. The quantification of vinculin-positive focal adhesions was done according to a protocol published previously [48].

2.7.2. Cell growth assay

Qblue assay was used as an indicator of cellular viability and cell growth. Cells were seeded at a density of 20.000 cell·mL^{-1} in DMEM 10% FCS and incubated at 37°C/ 5% CO_2 for 24, 48, and 72 h for the first, second and third well-plate, respectively. QBlue reagent was mixed with colorless DMEM to produce a 10% (*v*/v) solution. The DMEM was removed from cells well-plate and the 10% solution of QBlue assay was added. The cells were incubated with 300 μL of the solution at 37°C/ 5% CO_2 for 3 h. After incubation, 100 μL was collected from each sample and transferred to 96 well-plates trice. The samples were analyzed using the microplate reader (FLUOstar OPTIMA, BMG LabTech, Germany) which was adjusted to a wavelength of 544 nm for excitation and 590 nm for emission.

Table 1
Primers of target and housekeeping genes.

Symbol	Name	Assay ID
Osteoblast		
ALP	Alkaline phosphatase	qMmuCEP0027961
RUNX2	Runt-related transcription factor-2	qMmuCEP0057696
NOG	Noggin	qMmuCEP0058332
SP7	Osterix	qMmuCED0039982
Chondrocyte		
SOX9	Transcription factor SOX-9	qMmuCEP0053111
ACAN	Aggrecan	qMmuCEP0055269
COL1A1	Collagen type 1 alpha 1	qMmuCEP0052648
COL2A1	Collagen type 2 alpha 1	qMmuCEP0055155
Housekeeping gene RPLP0	60S acidic ribosomal protein P0	qMmuCEP0042968

2.8. Differentiation studies: osteogenesis

2.8.1. Alizarin red-S staining

C3H10T1/2 cells were seeded on PEM modified glass coverslips in 24 well plates at a density of 4×10^4 mL^{-1}. The cells were cultured on glass in presence of **osteogenic medium** as a positive control (DMEM 10% FCS, 100 nM Dex, 50 μg mL^{-1} ascorbic acid, and 10 mM β-Glycerophosphate), while the **basal medium** was DMEM with 10% FCS (negative control). The medium for the sample group was osteogenic medium without Dex. The Alizarin red (Carl Roth GmbH, Karlsruhe, Germany) staining was performed after 21 days as reported previously [46].

2.9. Differentiation studies: chondrogenesis

2.9.1. Safranin O staining

C3H10T1/2 cells were seeded on the samples placed into 24 well plates at high density of 1×10^5 mL^{-1}. Here, the chondrogenesis requires high density to induce cell-cell interactions similar to the precartilage condensation [49]. The cells were incubated in presence of a **chondrogenic medium** as a positive control (DMEM 10% FCS, 100 nM Dex, 5 μg mL^{-1} ascorbic acid) while **basal medium** was DMEM with 10% FCS (negative control). The medium for the samples group was chondrogenic medium in the absence of Dex.

The cells were prepared and fixed as described in Section 2.8. After removing paraformaldehyde, samples were washed twice with distilled water and incubated in 1% acetic acid for 15 s. Subsequently, the samples were incubated for 15 min with 0.1% safranin O solution (Sigma-Aldrich, Steinheim, Germany). After the incubation time, the samples were washed with PBS and studied with a microscope equipped with a camera (Axiovert 100, Carl Zeiss, Oberkochen, Germany).

2.10. RNA extraction and quantitative real-time PCR

C3H10T1/2 cells were seeded on glass coverslips coated with PEM coatings as in the previous section. The re-suspend cells were seeded on the samples in DMEM supplemented with 10% FCS at a density of 5×10^5 mL^{-1} for osteogenic and 1×10^6 mL^{-1} for chondrogenic differentiation. The composition of media was the same as described above. To evaluate the osteogenic and chondrogenic differentiation, the cells were incubated for 14 days.

The RNA was extracted from samples using TRIzol method (Invitrogen, Darmstadt, Germany) according to the manufacturer's recommended procedure. First, cDNA was synthesized using an iScript Advanced cDNA Synthesis Kit for RT-qPCR (Biorad, Hercules, CA, USA) in 20 μL reactions, according to the manufacturer's instructions.

qRT-PCR was performed under standard enzyme and cycling conditions on a CFX Connect real-time PCR Detection System (Biorad, Hercules, CA, USA). Primer sets were pre-validated by PrimePCR Probe Assays from Biorad (Hercules, CA, USA) for osteogenic genes (ALP, RUNX2, Noggin, and Osterix) and chondrogenic genes (SOX-9, ACAN, collagen alpha 1, and collagen type 2 alpha 1). The housekeeping gene RPLP0 was also used in this study (Table 1). Data analysis was performed using the BioRad CFX Manager Software 3.0 (Hercules, CA, USA). The conditions of qRT-PCR were as follows: 95 °C for 30 s followed by 39 cycles at 95 °C for 15 s and 60 °C for 30 s. The relative expression levels for each gene were calculated and normalized to the housekeeping gene RPLP0 by the DDCt method ($2^{-\Delta\Delta Ct}$) [50].

2.11. Immunohistochemical staining

C3H10T1/2 cells were seeded on glass coverslips coated with PEM coatings as described in the previous section of differentiation studies. To study the osteogenic and chondrogenic differentiation, the cells were incubated for 21 days. After the incubation time, cells were fixed using 4% paraformaldehyde (Sigma-Aldrich) solution at room temperature for

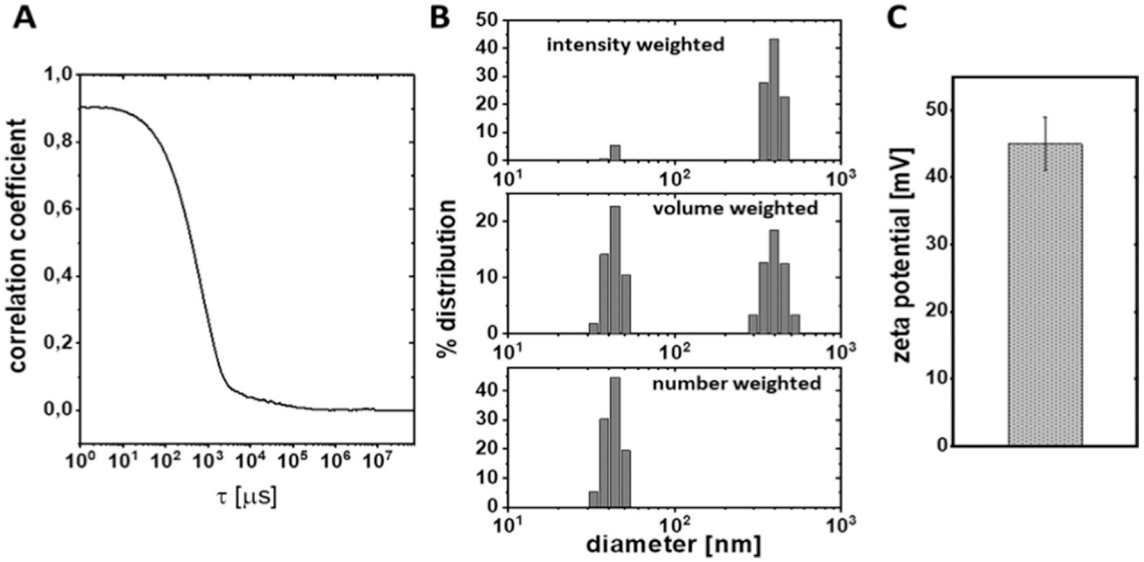

Fig. 2. Characterization of cationic liposomes loaded with Dex in acetate buffer pH 4 (10 mM, 0.15 M NaCl). (A) the correlation coefficient, (B) intensity, volume, and number weighted size distribution, (C) zeta potential (mean and standard deviation of three independent liposome preparations) measured by DLS and lDv.

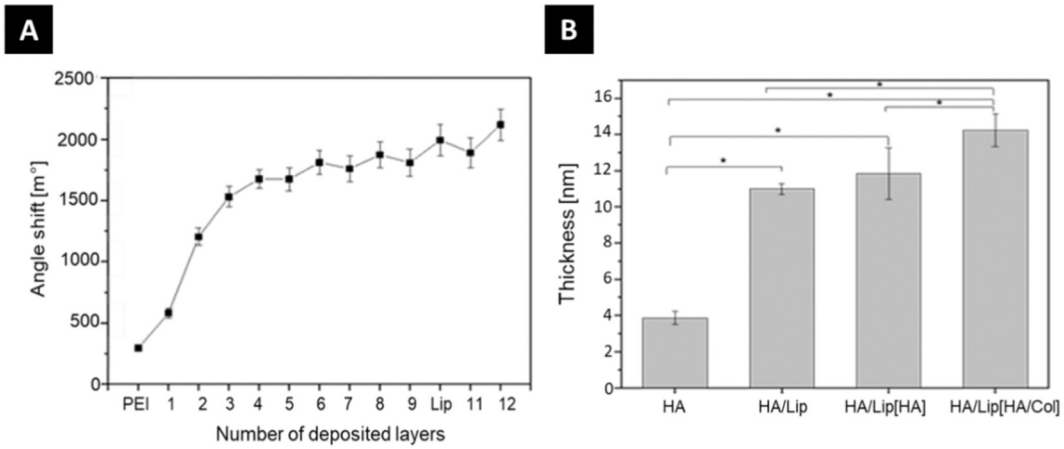

Fig. 3. (A) Layer growth of PEM systems of $[HA/Col]_4$ HA/Lip [HA/Col] by SPR numbered as 1 to 12 (1st layer to 12th layer). Odd layer numbers correspond to HA coating and even layer numbers correspond to Col coating except the 10th layer, which corresponds to liposomes loaded with Dex (Lip); $n = 20$, mean ± SD. (B) Progression of the layer thickness of PEM sequence $[HA/ Col]_4$ after adsorption of the additional layers of liposomes (Lip), hyaluronic acid (HA), and collagen I (Col) (see sequence details at the x-axis) determined by ellipsometry; $n = 10$, mean ± SD, $^*p \leq 0.05$.

15 min and washed three times with PBS. After permeabilization using 0.1% (*v*/v) Triton X-100 (Sigma-Aldrich) for 10 min, the non-specific binding sites were blocked with 1% bovine serum albumin solution (BSA, Carl Roth GmbH, Karlsruhe, Germany) in PBS at room temperature for 1 h. For visualization of chondrogenic markers, the cells were incubated with primary monoclonal antibodies raised against collagen type II (rabbit, Santa Cruz Biotechnology, Heidelberg, Germany) and a secondary antibody CY3 (anti-rabbit, Dianova, Hamburg, Germany) and ACAN (mouse, Santa Cruz Biotechnology, Heidelberg, Germany) and conjugated secondary CY2 (anti-mouse, Dianova, Hamburg, Germany). For detection of osteogenic markers, the cells were incubated with primary monoclonal antibodies raised against Col (mouse, Santa Cruz Biotechnology, Heidelberg, Germany) with secondary antibody anti-mouse (CY2) and (mouse, Santa Cruz Biotechnology, Heidelberg, Germany) with conjugated secondary anti-rabbit (CY3). The images were visualized using confocal laser scanning microscopy (CLSM 701, Carl Zeiss Micro-Imaging GmbH, Jena, Germany) using 20× and 63× oil immersion objectives. Images were processed with the ZEN 2008 software (Carl Zeiss).

2.12. Statistical analysis

All statistical analysis was performed with Origin 8G software. Mean, standard deviation, and analysis of significance were performed by one-way ANOVA (indicated as *). A value of $p < 0.05$ was considered as significantly different. Further, box-whisker diagrams are shown where appropriate. The box indicates the 25th and 75th percentiles, the median (dash), and the mean value (black square), respectively.

3. Results and discussion

3.1. Characterization of liposomes

The peptide-mimicking lipid OO4 bears ionizable amino functions and has an apparent pKa value of 6. The liposomes prepared solely from this lipid have a positive zeta potential over a wide pH range [51,52]. A positive charge of liposomes is needed for efficient embedding in LbL-based PEM formation. Here, the utilized liposomes are composed of a binary mixture of OO4/DOPE 1/3 (n/n). DLS and zeta potential measurements were performed to characterize the size and charge of the liposomes under conditions used for LbL. The results are presented in Fig. 2.

The autocorrelation function (Fig. 2A) demonstrates the high quality of DLS data with an intercept at 0.9, a sigmodal decay of the signal, and the absence of a noisy baseline which would indicate aggregation. The fitting of the autocorrelation function results in a bimodal size distribution curve (intensity weighted curve in Fig. 2B). The first size population is at diameter (d) ≈ 40–50 nm and a second one at d ≈ 300–500 nm. The size differences between both populations make it difficult to get quantitative information because the scattering intensity is approximately proportional to d^6. As such, the intensity distribution can be somewhat misleading, in that a small number of larger particles can dominate the distribution. Therefore, volume and number weighted size distribution curves were calculated, demonstrating that the 40–50 nm population is in a much higher quantity than expected from the intensity weighted curve [53]. In addition, zeta potential measurements show that the liposomes possess a positive surface charge required for immobilization on the PEM (Fig. 2C). DOPE is used as zwitterionic co-lipid in the mixture to decrease the charge density of the liposomes. This becomes obvious comparing the high zeta potential of OO4 liposomes ($\zeta > 40$ mV) with the liposomes OO4/DOPE ($\zeta = 30$ mV) [24,51]. Furthermore, DOPE increases the fusogenic character of liposomes in acidic milieus and therewith triggers endosomal escape of payload after endocytosis, a phenomenon often discussed for lipid-mediated nucleic acid transfer [54].

3.2. Physical characterization of multilayers

SPR was used to investigate the layer deposition of PEM in situ. Fig. 3 (A) shows a linear growth behavior of PEM system until the third layer. During the further deposition steps, the layer growth was reduced pronouncedly. Every deposition step changes the angle shift, which corresponds to the absorbed mass of each layer [13,55]. However, after the 4th layer the mass adsorption reached an equilibrium which was well in line with previous studies [56]. Furthermore, the addition of liposomes as the 10th layer (PEM sequence [HA/Col]4HA/Lip) resulted in an additional mass deposition (angle shift increased from ~1700 to 2000 m°). The deposition of a further bilayer of HA/Col causes a further small increase of angle shift, which indicates the deposition of both polyelectrolytes.

To obtain more information about liposome deposition, the PEM layer thickness was measured by ellipsometry. This measurement was conducted with duplicates of dry films on a silicon substrate at 5 different spots per film (n = 10). Fig. 3 shows an increasing thickness of PEM from 4.1 ± 0.2 nm for the sequence $[HA/Col]_4HA$ up to 14.2 ± 0.1 nm for the sequence $[HA/Col]_4HA/Lip[HA/Col]$ which is related to the increase of the number of layers of PEM. It is visible that the adsorption of liposomes makes the main contribution to the observed increase of

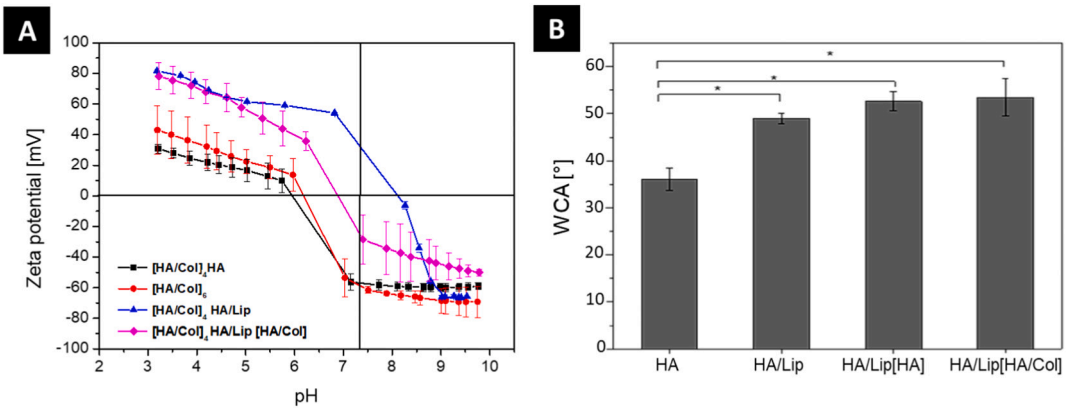

Fig. 4. A) Zeta potential measurements of the three different multilayers. Results represents means ± SD of two independent experiments. B) Static water contact angle (WCA) measurement during multilayer formation. The x-axis demonstrate the film composition deposited on the basal part $[HA/Col]_4$. Results represent means ± SD, $*p \leq 0.05$ of three independent experiments.

PEM thickness. However, the relatively low thickness after adsorption of liposomes compared to their size obtained in DLS is a consequence of the drying procedure which results in the shrinking by the loss of the encapsulated aqueous core of liposomes [57]. Hence, it can be assumed that the thickness of hydrated multilayers is considerably larger compared to the thickness of dry layers because also HA tends to absorb water leading to swelling of PEM [58]. The ellipsometry results confirm the increase in mass deposition observed with SPR, particularly after liposomes were added.

Moreover, the surface topography was evaluated by atomic force microscopy (AFM). In previous studies, Zhao et al. showed the topography of HA/Col PEM which displayed a smooth surface with a small number of short collagen fibrils [13]. The AFM studies shown in Fig. S1 confirm the previous data showing a smooth surface with a roughness average (Ra) of 1.731 ± 0.721 nm and root mean square roughness (Rq) 2.914 ± 1.698 nm (see Table S1). After the deposition of the liposomes [HA/Col]4HA/Lip an increment of the roughness to Ra 17.96 ± 6.219 nm and Rq 23.55 ± 7.66 nm can be seen in Table S1. Also, the images in Fig. S1 provide evidence that the liposomes are immobilized on the surface visible by the presence of round structures covering the whole surface area. The roughness value for the sequence [HA/Col]4HA/Lip [HA/Col] are Ra 11.64 ± 2.647 nm and Rq 15.23 ± 3.389 nm. The values indicate the presence of the liposomes after deposition of additional bilayer where the liposomes changed their morphology and elongate diameter showing a rather flat structure on the surface due to the flexibility of liposomes and the strong Coulomb attractive force to the deposited polyanion HA [46,57]. The structures are also maintained after deposition of an additional bilayer of HA/Col.

The knowledge of surface charge after each deposition step represents an important characterization of the buildup process of PEM [59]. Surface charge density, which corresponds to zeta potential, has also a pronounced effect on cell adhesion and fate [60]. Previous research has shown that PEM zeta potentials, particularly those made of hydrophilic biopolymers, reflect not only the charge distribution of the last polyelectrolyte layer but also of preceding ones due to the existence of swollen, conductive surface layers [61]. Fig. 4A shows the zeta potential of the final PEM and intermediate PEM assemblies as a function of pH value adjusted during the titration process. The pKa value of Col is around 5.5 [55]. Hence, it can be assumed that the Col is positively charged at low pH during titration and the charge will decrease continuously with increasing the pH value. In contrast, HA carries a negative net charge due to the presence of carboxylic groups with a pKa of 2.9 [62], which will further decrease the zeta potential when the pH value is increased during titration. The zeta potential of $[HA/Col]_6$ multilayers (curve with red points) shifts from positive values in the acidic to negatives potentials in the basic pH region. This indicates the contribution of both charged species, such as Col at low pH and HA at high pH to the zeta potential, related to the fact that not only the outermost layer but also inner layers of PEM contribute to the zeta potential as detected by Zimmermann & Werner [61,63]. The addition of a further layer of HA to $[HA/Col]_4$ (curve with black squares) decreases the zeta potentials slightly and indicates the contribution of the

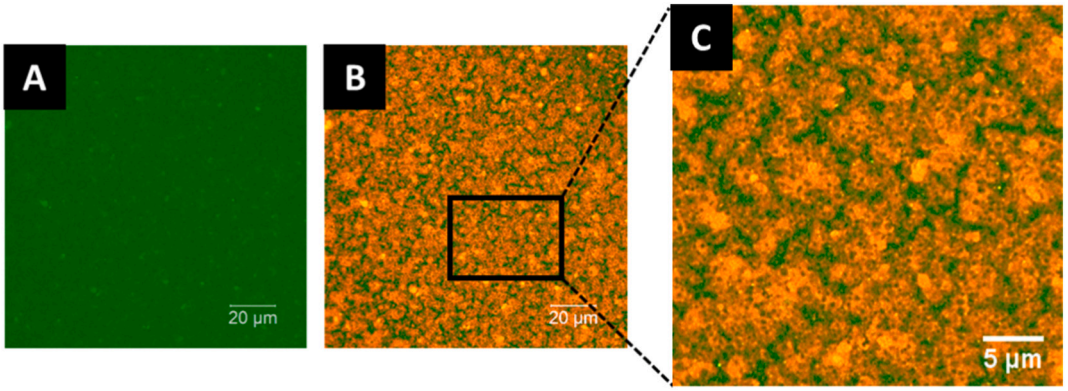

Fig. 5. CLSM images of PEM system after deposition of the liposomes: $[HA\text{-}FITC/Col]_4HA/Lip[HA\text{-}FITC/Col]$ HA was labeled using FITC (green), liposomes with Rhodamine-DOPE conjugated (red) on PEM. A) FITC fluorescence distribution, B) merged image of FITC fluorescence and Rhodamine-DOPE fluorescence C) detail (black square in B) merged image of HA and liposomes distribution of the area in the black square [scale 20 µm and 5 µm]. (For interpretation of the references to colour in this figure legend, the reader is referred to the web version of this article.)

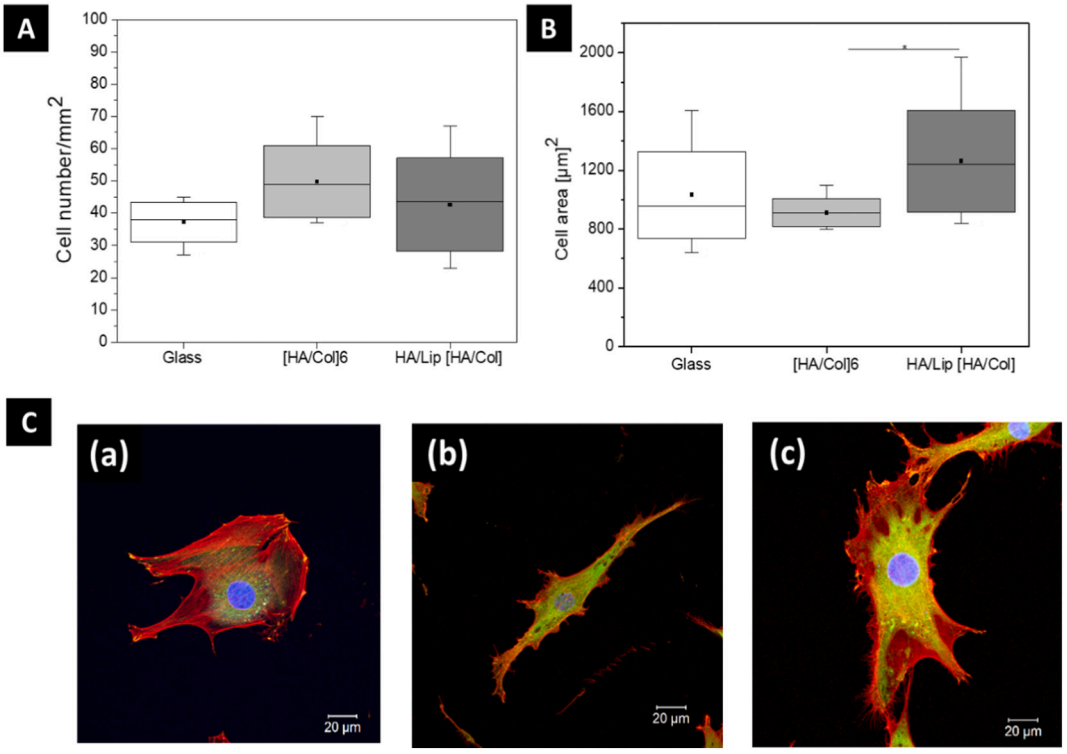

Fig. 6. A) Quantification of cell count per square millimeter B) Cell spreading area (μm^2) on each of the multilayers after 4 h; samples: Glass, $[HA/Col]_6$, $[HA/Col]_4$* HA/Lip [HA/Col] (Box plots with whiskers, representing first and third quartiles, medians and means). (*) statistically significant with a *p*-value $\leq$0.05. C) Merged CLSM image of adherent C3H10T1/2 cultured on the different PEM after 4 h of incubation in serum and serum-free medium. (a) Glass, (b) $[HA/Col]_6$, (c) $[HA/Col]_4$ HA/Lip[HA/Col]. The cells are stained for filamentous actin (red), vinculin-positive focal adhesions (green), and nucleus (blue). [Scale 20 µm]. (For interpretation of the references to colour in this figure legend, the reader is referred to the web version of this article.)

polyanion HA to the potential. The adsorption of liposomes $[HA/Col]_4$HA/Lip (blue triangles) leads to a dramatic increase of zeta potentials with a huge shift of point of zero charge (PZC) from pH 6 to pH 8.5 which represents the positive charge of the cationic liposomes. The coverage of the liposome layer with an additional bilayer of HA/Col decreases the zeta potential again, but it remains still higher than that of the $[HA/Col]_4$ HA, which indicates that the liposomes underneath make still a contribution to the zeta potential of the system. The PZC of this system is 6.8, which means that both anionic and cationic species contribute to the potential. The zeta potential measurements show clearly that liposomes adsorb on the $[HA/Col]_4$HA multilayers and they remain also when an additional bilayer of HA/Col is immobilized on top of them.

On the other hand, surface wettability is another important factor that can affect the biological response to an implant because it affects protein adsorption and cell adhesion [64]. Fig. 4 (B) shows that $[HA/Col]_4$HA is hydrophilic with a WCA of ~35°, which is related to the fact that HA is a hydrophilic polysaccharide [13]. After the adsorption of liposomes on PEM $[HA/Col]_4$HA/Lip, the WCA increased to a value of 50°, which corresponds to a moderately wettable surface due to the presence of amino groups, which make WCA in this range [65]. The subsequent $[HA/Col]_4$HA/Lip/HA displays an angle of ~53°, and the final PEM $[HA/Col]_4$HA/Lip[HA/Col] was characterized by a WCA of ~55°, demonstrating that the wetting properties of liposomes are also dominant after deposition the final bilayer, which indicates an intermingled structure of liposomes and polyelectrolytes in the outermost layer of the system [66].

Further evidence for the entrapment of liposomes in the PEM system is shown in Fig. 5 presenting micrographs made by CLSM. Fig. 5 A shows a uniform distribution of HA labeled with FITC in the PEM [HA-FITC/Col]$_4$HA/Lip[HA-FITC/Col] (green colour). Fig. 5B) displays the distribution of Rhodamine-DOPE fluorescence across the PEM (orange colour), with higher magnification in Fig. 5 C demonstrating the presence of labeled liposomes. The image depicts the distribution of liposomes over the entire area; however, the image indicates the presence of some liposomes aggregates and a partially homogeneous distribution, which could be due to interactions between the positive surface charge of the liposomes and the layer arrangement with carboxylic groups of HA and Col fibrils.

3.3. Adhesion and growth of C3H10T1/2 cells

C3H10T1/2 cells are a well-characterized model for in vitro differentiation of multipotent cells into osteoblasts, chondrocytes, and adipocytes [39,40]. The cell adhesion studies were carried out by the quantification of cell number and cell area including visualization of actin filaments (red staining), vinculin-positive focal adhesions (green staining), and nuclei (blue staining). These studies are important to understand how the PEM system properties influence cell adhesion, which may have also an effect on subsequent cell differentiation [67]. Fig. 6 A shows a higher number of cells on the PEM surfaces compared to the cells on glass used as a control after 4 h, which is due presence of cell receptors for HA and Col. Further, the cells seeded on PEM $[HA/Col]_6$ and $[HA/Col]_4$HA/Lip[HA/Col] show no significant difference probably due to similar composition of terminal layer (HA and Col). The quantification of the cell area (Fig. 6 B) demonstrated a significant higher spreading of cells on $[HA/Col]_4$HA/Lip[HA/Col] related to its higher WCA and zeta potential in contrast to the control and the basal PEM $[HA/Col]_6$. Fig. 6 C demonstrates the organization of the actin filaments on the different substrates. The cells on glass were characterized by a small aspect ratio of an irregular form and the actin filaments were organized mostly circumferentially. The cells cultured on the basal system $[HA/Col]_6$ had a longitudinal distribution of the actin filaments. However, the cells on $[HA/Col]_4$HA/Lip[HA/Col] displayed an

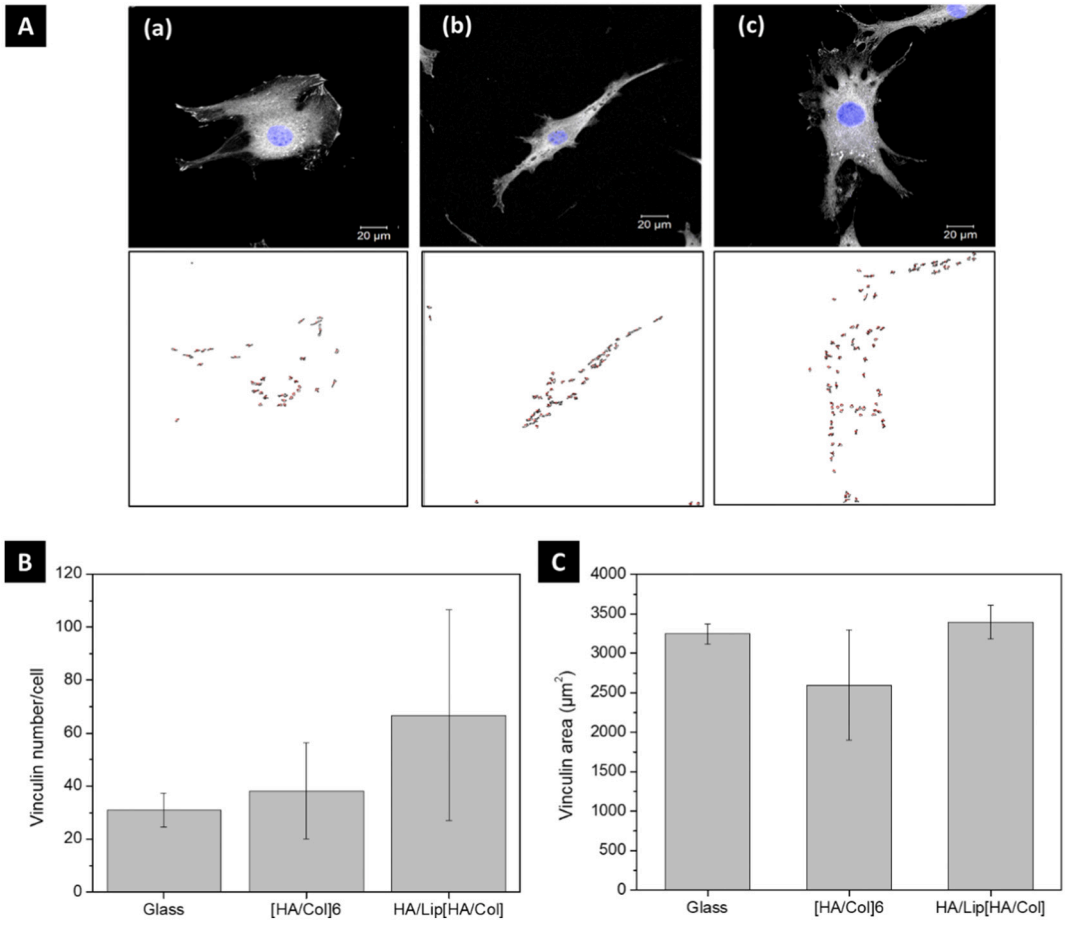

Fig. 7. A) Visualization of vinculin-positive focal adhesions in cells seeded on a) glass, b) $[HA/Col]_6$ and c) $[HA/Col]_4HA/Lip[HA/Col]$ B, C) Quantification of vinculin-positive focal adhesions number per cell and vinculin per cell area μm^2. vinculin-positive focal adhesions was quantified by Image J. Results represent means ± SD values, $n = 5$, $p \leq 0.05$.

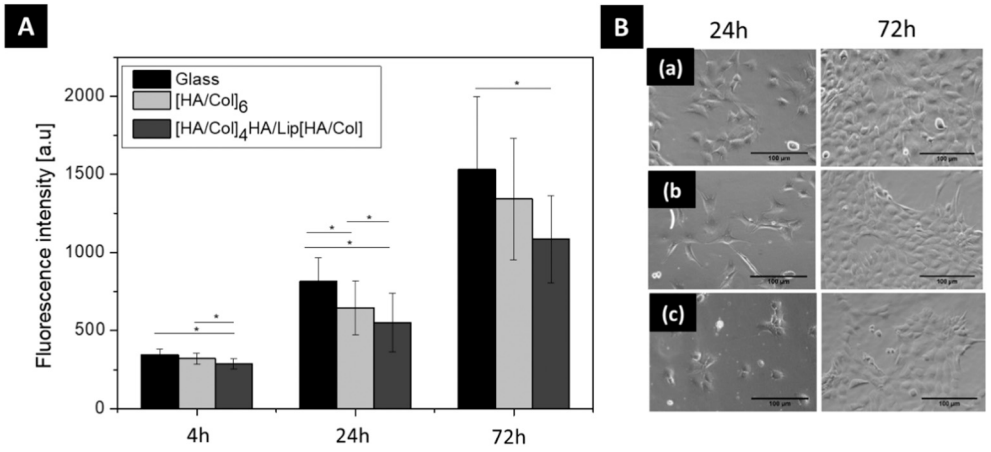

Fig. 8. A) Growth of C3H10T1/2 seed on glass and PEM system of $[HA/Col]_6$ and [HA/ Col]$_4$HA/Lip[HA/Col] measured by the QBlue assay after 4 h, 24 h, and 72 h. B) Phase-contrast images of cell seeding on glass and multilayers after 24 h and 72 h. (a) Glass, (b) [HA/Col]6, (c) $[HA/Col]_4HA/Lip[HA/Col]$. Scale bar 100 μm.

elongated and extended morphology which underlines that the embedded liposomes have a promoting effect on cell adhesion and spreading.

Fig. 7 displays the position of the vinculin-positive focal adhesions at the end of the actin filaments but also in central regions. Nevertheless, cell spreading was observed on both multilayers surfaces but the vinculin-positive focal adhesions amount was different. The PEM system of $[HA/Col]_4HA/Lip$ [HA/Col] showed a higher number and larger length of vinculin positive staining compared to the basal PEM [HA/ $Col]_6$. Vinculin reinforces focal adhesion by crosslinking actin filaments to the structure molecules like talin [68]. This is an important step in cellular mechanics linking the cell to its substrate. Also, vinculin is recruited in integrin-mediated adhesions and the actin cytoskeletal network that is connected to the ECM. Therefore, the presence of

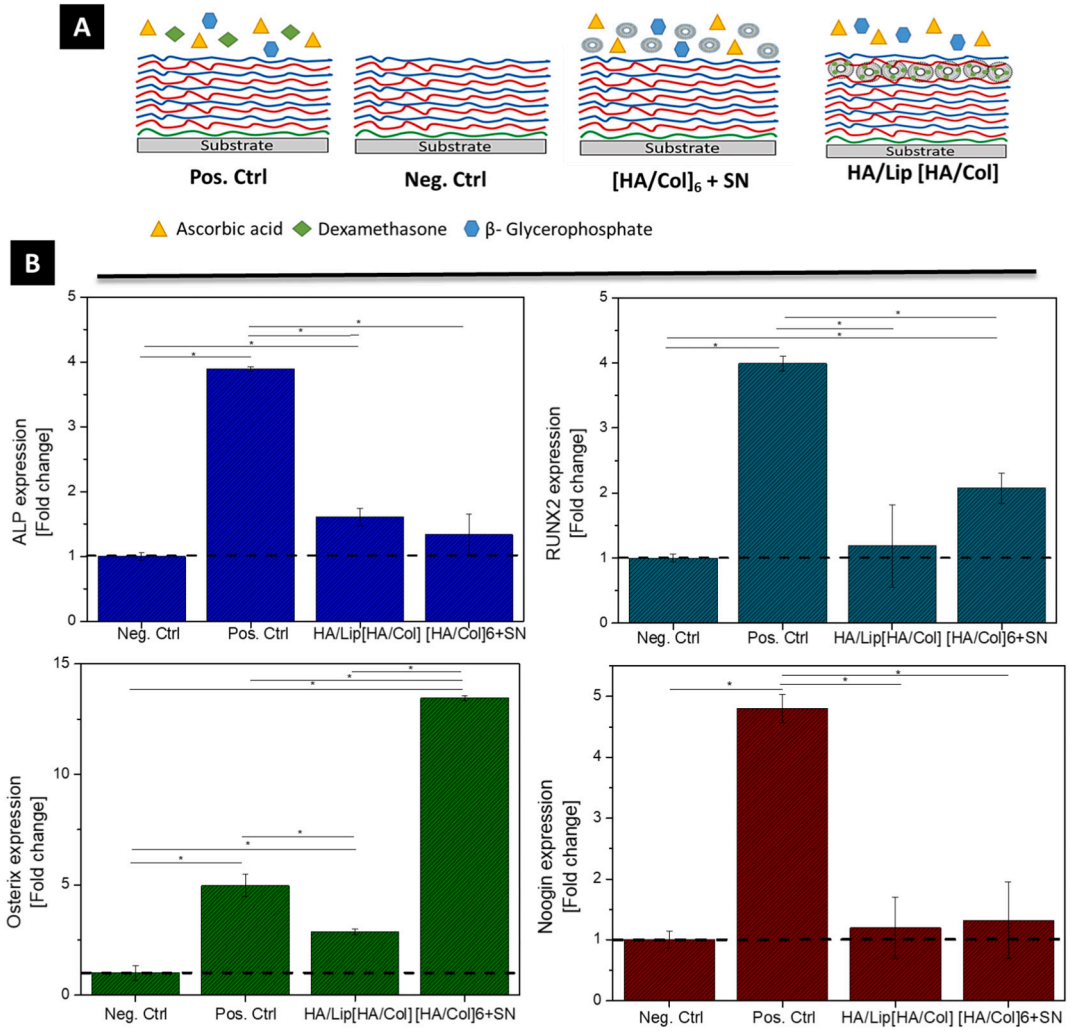

Fig. 9. A) Schematic illustration of the screened differentiation environments in the in vitro study. B) Relative expression of mRNA osteoblast markers (ALP, Runx2, Osterix, and Nogging) were determined after 14 days of incubation on PEM. qRT-PCR analyses were performed as described in the materials and methods. Data represent mean ± SD values, $n = 5$, $p \leq 0.05$ and Scheffe-Post-Hoc test.

vinculin-positive focal adhesions in the samples gives an indication of integrin ligation and signal transduction processes [69].

Growth of C3H10T1/2 cells was studied by QBlue assay evaluating their metabolic activity to assure that cells can survive and multiply during longer culture for chondrogenic and osteogenic differentiation (Fig. 8). For this assay the samples were divided into three groups: the control group of C3H10T1/2 cells was seeded on glass slides and compared with cells growing on $[HA/Col]_6$ and on $[HA/Col]_4HA/Lip$ [HA/Col]. In Fig. 8A it is shown that cells seeded on glass and both PEM system with liposomes showed similar metabolic activity after 4 h of incubation, which corresponds roughly to the results of adhesion studies. A significant increase within each group was detected with increasing time of culture certifying that cell can also grow on PEM as prerequisite for the differentiation studies. The positive control after 48 h and 72 h showed a higher fluorescence intensity, compared to $[HA/Col]_6$ and $[HA/Col]_4HA/Lip$ [HA/Col]. As can be seen in the Fig. 8 B, cells were able to grow on all substrata over the time. However, the glass sample shows higher cell growth might due to the stronger substrate stiffness in comparison with the soft hydrated PEM systems where the HA has high water uptake capability and will decrease stiffness and roughness of the substratum [58,70]. It is well know that MSCs on soft substrates decrease the proliferative activity compared to cells grown on stiffer surfaces [71]. This consequence might not affect cell viability in vivo, but only their proliferative capacity [72].

Protein adsorption and cell adhesion are affected by the surface charge and wetting properties of the material [73,74]. For instance, negatively charged surfaces inhibit cell attachment, whereas positively charged surfaces stimulate [60]. The PEM system of $[HA/Col]_4HA/Lip$ [HA/Col] showed positive zeta potential after the adsorption of the liposomes, where it is possible to observe a high cell area and a larger number of vinculin-positive focal adhesions compared to the basal sample $[HA/Col]_6$. In addition, the wettability of materials has been proven to have a considerable influence on cell growth and function [74]. The binding of liposomes and additional bilayer with Col a significantly increased WCA indicating a less hydrophilic surface. This reduction in the hydrophilicity decreases the hydration force of repulsion, promoting the cell adhesion process [50].

On the other hand, cell adhesion depends on the interactions of cells with their surrounding microenvironment, particularly ligands of different cell adhesion receptors [74]. HA and Col play important roles in the regulation of cell adhesion and spreading. For instance, HA can bind to a variety of cell surface receptors named hyaladherins, such as CD44 and RHAMM [75]. CD44 proteins are involved in a diversity of cellular functions, including growth and differentiation [75,76]. For Col, there are specific proteins that play a key role in this process, called integrins. The integrin family contains four collagen receptors such as α1β1, α2β1, α10β1 α11β1, whereas α2β1 integrin is the main receptor for Col [77]. Therefore, both samples of PEM systems present a higher

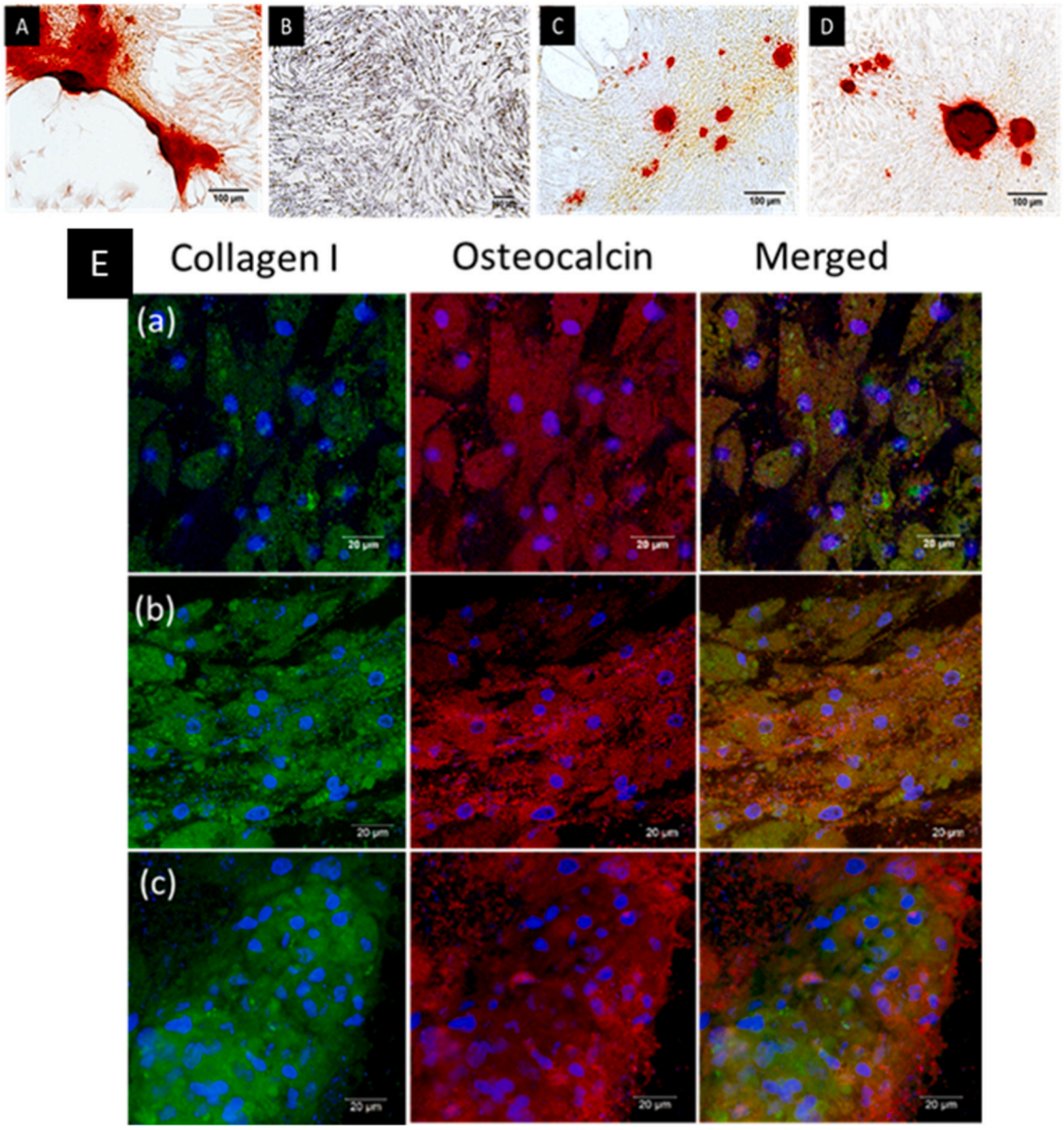

Fig. 10. Histochemical staining of C3H10T1/2 cells cultured on various test samples with basal medium and osteogenic medium. A) Positive control, $[HA/Col]_6$, B) Negative control, $[HA/Col]_6$ basal medium, C) $[HA/Col]_6$ and liposomes in the supernatant, D) $[HA/Col]_4HA/Lip[HA/Col]$. Alizarin red staining was performed after 21 days. Calcium deposits were staining in red [scale 100 μm]. E) CLSM images of immunofluorescence staining of collagen I and osteocalcin of C3H10T1/12 cells cultured in osteogenic medium after 21 days. a) Positive control, $[HA/Col]_6$, b) $[HA/Col]_6$ and liposomes in the supernatant, c) $[HA/Col]_4HA/Lip$ [HA/Col]. Collagen I (green fluorescence), osteocalcin (red fluorescence), nuclei (blue fluorescence) Scale bar 20 μm. (For interpretation of the references to colour in this figure legend, the reader is referred to the web version of this article.)

number of vinculin-positive focal adhesions unlike the control (glass) due to the presence of fibrillary collagen as a terminal layer promoting the cell adhesion via integrin α2β1 receptor of Col [52]. The benefit of integrin-binding surfaces is an enhanced cell adhesion and expansion [78]. For instance, integrins are of focal adhesion complexes that contain linker proteins to the cytoskeleton like, talin, and α-actinin and signaling transducers like vinculin and focal adhesion kinase [79]. These focal adhesions are involved in the adhesion process, function as the structural link between the cytoskeleton and ECM and activate signaling pathways to regulate transcription factors, involved in cell growth and cell differentiation [79,80].

3.4. Osteogenic differentiation of C3H10T1/2 cells

Previous studies confirmed that the cationic OO4/DOPE liposomes embedded in a PEM system can be used for controlled release or transfer of compounds into cells [46]. To induce cell differentiation, Dex was incorporated in the lipid bilayer of the liposomes as described in the Materials and methods section. Dex activates the expression of Runx2 which acts as an expression factor for procollagen [38]. Further, Dex in combination with ascorbic acid (ASC) and ß- glycerophosphate (β-Gly) has shown to regulate the osteogenesis of mouse MSCs with mineralization in vitro [44]. To determine if there were levels of osteogenic markers due to Dex effects on cells, the relative quantification of mRNA was performed by qRT-PCR after 14 days in a growth medium with ASC and β-Gly. The different conditions are represented in Fig. 9A. The qRT-PCR results (Fig. 9 B) demonstrated that Dex in the medium (positive control) or encapsulated in liposomes resulted in an upregulation of the gene expression of osteogenic markers (ALP, Runx2, osterix, and noggin) compared to the negative control, which was not treated with

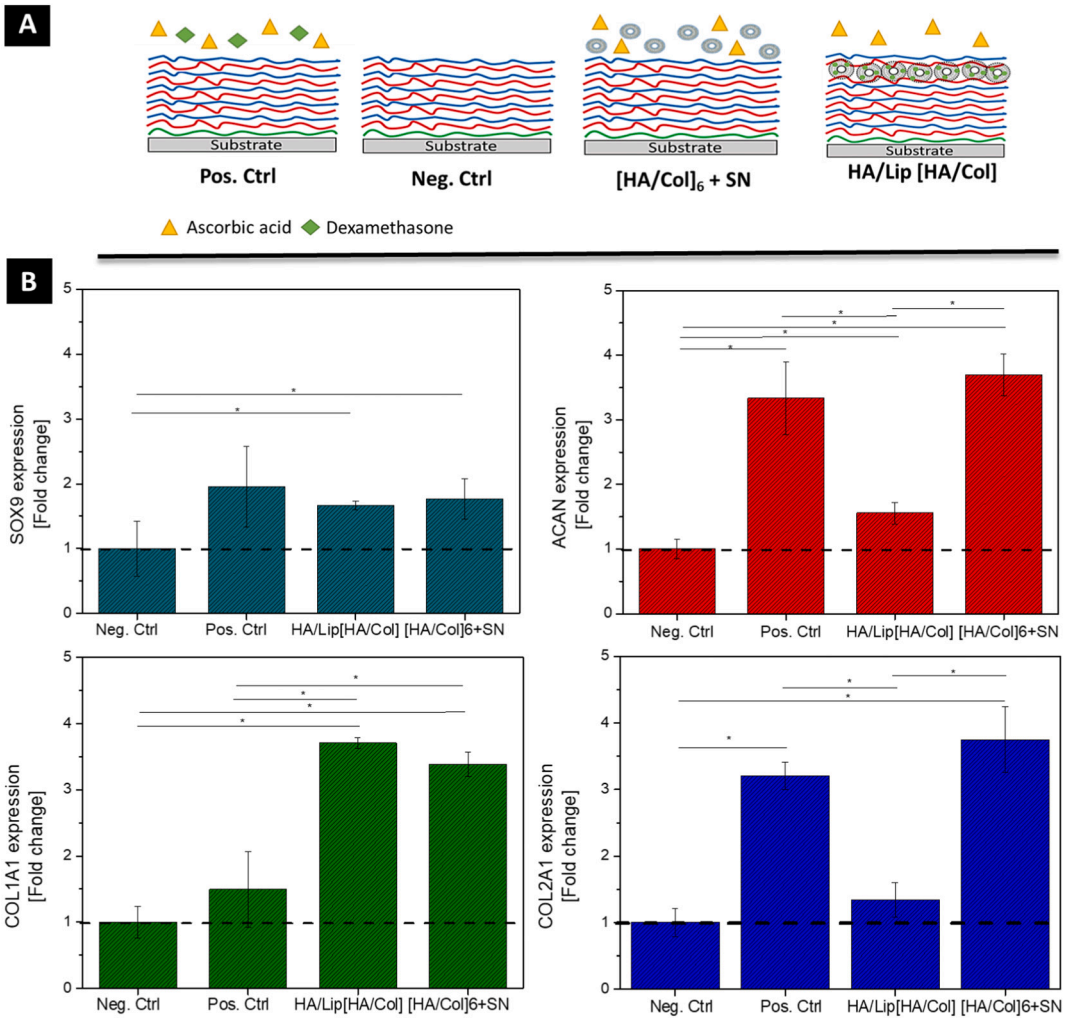

Fig. 11. A) Schematic illustration of the screened differentiation environments in the in vitro study. B) Relative expression of mRNA chondrogenic markers (Sox9, ACAN, Col1A1, and Col2A1) were determined after 14 days of incubation on PEM. qRT-PCR analyses were performed as described in the materials and methods. Data represent mean ± SD values, $n = 5$, $p \leq 0.05$ and Scheffe-Post-Hoc test.

Dex. In addition, a higher level of ALP was found on the liposomes embedded into PEM. The high-level expression of ALP can be found because ALP is an early marker in osteogenesis and it promotes the formation of hydroxyapatite crystals in the bone matrix [81]. However, it is possible to observe an increase of other osteogenic markers like Runx2 and noggin (compared to negative control), but the expression of mRNA was lower compared to the positive control. Another important transcription factor is osterix. This transcription factor activates genes during the differentiation of pre-osteoblast to the final stage that is osteocytes [82]. In addition, Sox9, Runx2, and osterix play an important role in the decision by which the cells differentiate to osteoblast or chondrocytes [83]. The qRT-PCR shows increased expression levels in both systems with Dex-loaded liposomes. Further, the expression of the markers where the liposomes were added in the supernatant (SN) was high, which might be to the direct contact of the liposomes with the cell, compared to the liposomes embedded in the film. For that reason, to confirm the qRT-PCR results, the deposition of calcium phosphate at 21 days was studied by Alizarin red staining (Fig. 10 A).

This result is supported by the images obtained of C3H10T1/2 culture after histochemical staining by Alizarin Red S that interact with hydroxyapatite and results in red staining of mineralized nodules that corresponds to an ECM rich in calcium phosphates. These nodules were observed when cells were cultured in $[HA/Col]_4HA/Lip[HA/Col]$ and liposomes in the supernatant $[HA/Col]_6$ + SN in presence of the osteogenic medium. These results confirm the previous data of qRT-PCR.

Another method to evaluate the osteogenic differentiation was through immunofluorescence staining of Col and OCN after 21 days of incubation (Fig. 10E). The positive staining confirmed the presence of Col and OCN, which are specific protein markers synthesize by osteoblast during maturation [84]. The presence of markers was found in both of PEM systems $[HA/Col]_4HA/Lip[HA/Col]$ and liposomes in the supernatant $[HA/Col]_6$ + SN. These results confirmed the protein production of osteogenic proteins at later stages but also supported that the liposomes with Dex can induce osteogenic differentiation.

On the other hand, connective tissues cells differ importantly in phenotype. The shape of MSC is involved in their specialized function, while at the same time drive to their multicellular organization [85]. For instance, cell spreading enables osteogenic matrix deposition during bone formation and these differences in cell morphology are due to the changes in the expression of the integrins, cadherins, and cytoskeletal proteins [67]. McBeath et al, demonstrated that cell spreading increased osteoblast differentiation in preosteoblastic progenitors [67]. Thus, previous results showed a high spreading presence in the PEM system $[HA/Col]_4HA/Lip[HA/Col]$ in which not only the Dex is involved in the differentiation, but also the spreading phenotypes of cells are related to osteogenic differentiation. In contrast, for chondrogenesis, the cells need to grow at high densities where the cell spreading on the surface decreases but cell-cell contact and paracrine signaling increase [67].

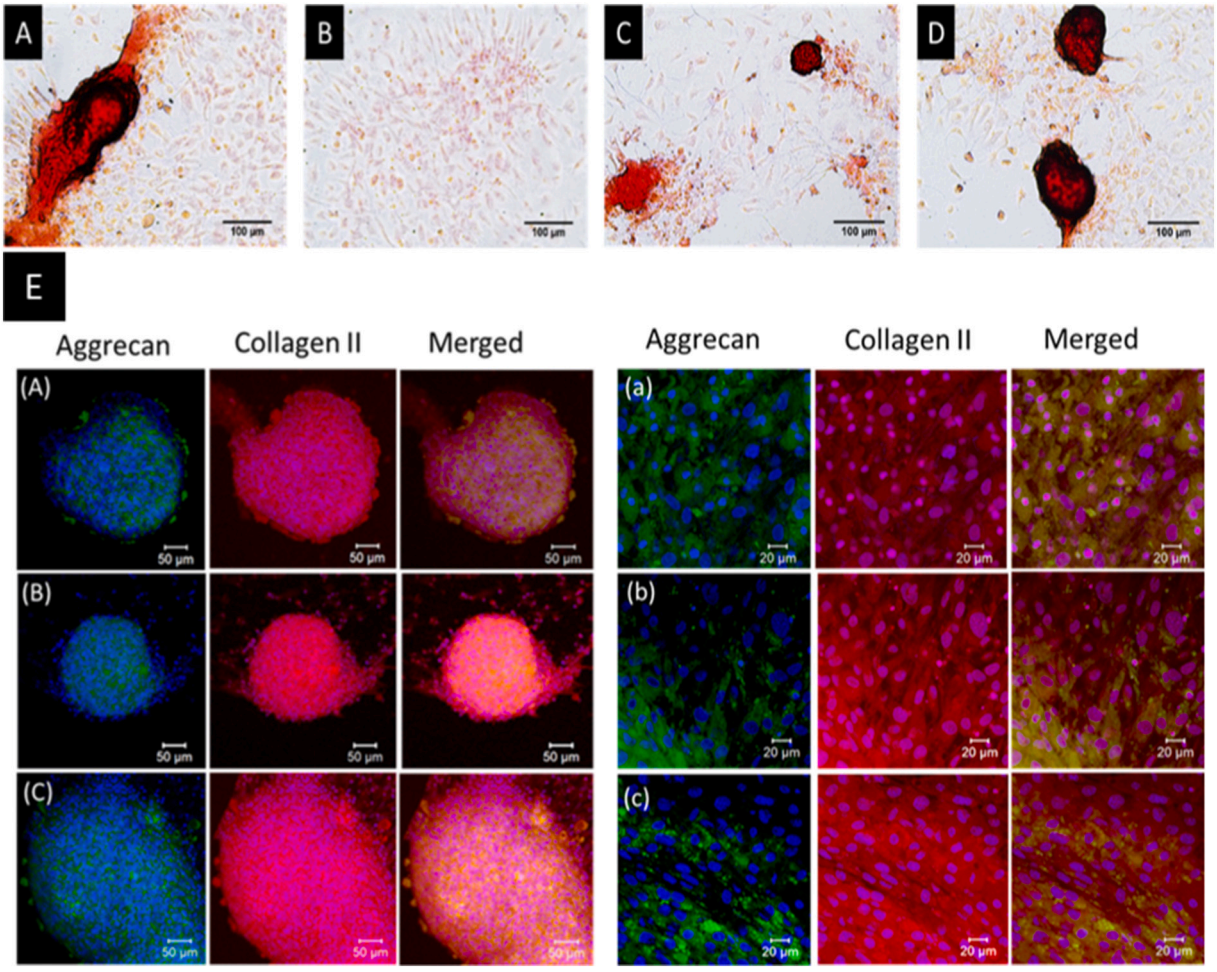

Fig. 12. Histochemical staining of C3H10T1/2 cells cultured on various test samples with basal medium and chondrogenic medium. A) Positive control, $[HA/Col]_6$, B) Negative control, $[HA/Col]_6$ basal medium, C) $[HA/Col]_6$ and liposomes in the supernatant, D) $[HA/Col]_4$ HA/Lip [HA/Col]. Safranin O staining was performed after 21 days. Accumulation of glycosaminoglycans was staining in red [scale 100 μm]. E) CLSM images of immunofluorescence staining of aggrecan and collagen II of C3H10T1/12 cells cultured in the chondrogenic medium after 21 days. A, a) Positive control, [HA/Col I]$_6$, B, b) $[HA/Col]_6$ and liposomes in the supernatant, C, c) $[HA/Col]_4$ HA/Lip [HA/Col]. Aggrecan (green fluorescence), collagen II (red fluorescence), nuclei (blue fluorescence). Left images: scale bar 50 μm. Right images: scale bar 20 μm. (For interpretation of the references to colour in this figure legend, the reader is referred to the web version of this article.)

3.5. *Chondrogenic differentiation of C3H10T1/2 cells*

Dex not only induces the Runx2 expression but can also be involved in the expression of Sox9 for chondrogenesis. The orientation of chondrogenic differentiation is connected to osteogenesis since both processes share the transcription factor of Sox9 [42]. Some authors refer that Dex increases Sox9 expression in primary chondrocyte cultures, in which Sox9 controls collagen II a1 and ACAN gene expression [86]. However, the molecular mechanism by how Dex produces its effects is still unknown. The mesenchymal stem cells that go through chondrogenesis express proteins associated with hyaline cartilage such as ACAN and collagen type II [87,88]. For instance, hyaline cartilage is present on the articular surface of the bone with collagen type II as the main component of this cartilage, while fibro-cartilage is found on the meniscus containing fibers of Col [89]. The difference between these types of collagen is that Col forms heterotrimeric triple helices which are self-assembled and collagen type II forms homotrimeric molecules [90]. In addition, it is known that chondrogenic differentiation depends on cell density and the experimental system. Seeding the high density of cells can induce endochondral ossification due to the formation of dense cell-cell interaction regulated by N-cadherin's [49,91]. For that reason, chondrogenic markers such as Sox9, ACAN, Col, and collagen type II were measured by qRT-PCR after 14 days of incubation on the mRNA level. Fig. 11 A shows the different conditions that were used to induce chondrogenic differentiation and the PEM systems. Fig. 11B shows the presence of these chondrogenesis markers Sox9, ACAN, Col, and collagen II in cells when they were exposed to Dex. Here, the Dex is immediately available for the positive control and the liposomes in the supernatant in comparison with the liposomes embedded into PEM. However, the PEM systems $[HA/Col]_4HA/Lip[HA/Col]$ shows similar Sox9 values as the positive control and the liposomes in the supernatant [HA/Col I]$_6$ + SN compared to the negative control. This result is an indicator that the cells were induced to undergo chondrogenesis. There were also increased mRNA values for ACAN and collagen type II for the PEM systems $[HA/Col]_4HA/Lip[HA/Col]$, but the values of the positive control and the PEM system $[HA/Col]_6$ + SN were not reached. Col shows a high expression in both PEM systems, with liposomes in the SN and embedded in the PEM.

It is known that chondrogenesis can be stimulated in the presence of Dex and increase GAGs expression [88]. Therefore, histochemical staining with safranin O that detects acidic GAGs (e.g. hyaluronan, chondroitin sulfate, etc.) was done after 21 days. Fig. 12A–D shows the staining of the accumulation of GAGs and clusters with condensation of cells, which was positive for the control (positive) and both PEM systems with liposomes embedded or in the SN.

The study of chondrogenic markers by immunostaining revealed that

ACAN was uniformly distributed through the cell cluster and at the periphery, and collagen type II was accumulated also within the cluster in all the samples (Fig. 12). Here, the detection of ACAN and collagen type II confirmed the chondrogenic differentiation. In addition, previous studies demonstrate that the presence of HA and Col induces chondrogenic differentiation because of the partially mimic of ECM of bone and cartilage [39]. The mesenchymal progenitor shares Sox9 and the addition of induction supplements such as Dex and induce the differentiation to chondrogenic or osteogenesis. Further, transcription factor Sox9 can control the chondrocyte proliferation and the progression to hypertrophy chondrocytes and go through osteogenic linage [42,92].

In literature it was demonstrated that chondrogenesis is induced when cells are seeded in high density in vitro because this mimics the condensation during cartilage formation. Interestingly, the low cell density causes high cell spreading to induce osteogenic differentiation, however, for chondrogenic differentiation the high cell density decreases the cell spreading and increase the number of cadherins, and trigger chondrogenesis [93]. For that reason, the advantage of the [HA/Col]$_4$HA/Lip[HA/Col] system is that the cells can differentiate into both osteogenic or chondrogenic pathways with minor changes in the conditions.

4. Conclusion

The LbL technique can be used to create multifunctional surface coatings that can modify the composition and physicochemical properties of implants surfaces with liposomes adsorption to allow the delivery of compounds like Dex. This technique can develop ECM-inspired surface coatings for osteochondral implants to induce bone and cartilage differentiation. In previous studies [40], the PEM system and Dex-loaded liposomes demonstrated a uniform and stable adsorption with a successful transfer into cells to induce cell differentiation. The benefit of the immobilization of liposomes in PEM with a cover bilayer of HA/Col is to protect them from degradation and spontaneous release of Dex, reducing the systemic effects and having a local delivery. The PEM made of HA/Col with embedded liposomes provides also good cell adhesion which is an important for integration of implants related to cell growth and differentiation. An important point is probably the effect of combining adhesive cues by the ECM-like composition of PEM with chemical cues like Dex to activate pathways for cell differentiation. Hence, differentiation of C3H10T1/2 cells was more prominent on the PEM system with embedded Dex-loaded liposomes compared to the use of free liposomes in the SN. Overall, the combination of multilayers mimicking the matric of bone and cartilage in combination with Dex might be interesting for future studies as coatings for osteochondral implants.

CRediT authorship contribution statement

Brito-Barrera Y A: Conceptualization, Methodology, Visualization Investigation, Writing - Original Draft. **Husteden C:** Investigation, Visualization, Writing - Review & Editing. **Alherz J:** Investigation, Visualization. **Fuhrmann B:** Visualization, Supervision **Wölk C:** Conceptualization, Supervision, Validation, Writing - Review & Editing.: **Groth T:** Conceptualization, Supervision, Project administration, Writing- Reviewing and Editing.

Funding

Y.A.B.B supported by the CONACYT-México and German Academic Exchange Service (DAAD). The support by the Deutsche Forschungsgemeinschaft (DFG) project-ID [396823779] to C.W. is greatly acknowledged. TG acknowledges the kind support by the Ministry of Science and Higher Education of the Russian Federation within the framework of state support for the creation and development of World-Class Research Centers “Digital biodesign and personalized healthcare” [075-15-2020-926].

Declaration of competing interest

The authors declare that they have no known competing financial interests or personal relationships that could have appeared to influence the work reported in this paper.

Acknowledgments

The authors thank the technical assistance of Mrs. Marlis Porobin for performing zeta potential measurements.

Appendix A. Supplementary data

Supplementary data to this article can be found online at https://doi.org/10.1016/j.msec.2021.112516.

References

[1] Y. Lu, W. Zhang, J. Wang, G. Yang, S. Yin, T. Tang, X. Jiang, Recent advances in cell sheet technology for bone and cartilage regeneration: from preparation to application, international, J. Oral Sci. (2019), https://doi.org/10.1038/s41368-019-0050-5.
[2] A.M. Yousefi, M.E. Hoque, R.G. Prasad, N. Uth, Current strategies in multiphasic scaffold design for osteochondral tissue engineering: a review, 2015, https://doi.org/10.1002/jbm.a.35356. Wiley Online Library.
[3] W. Swieszkowski, B.H.S. Tuan, K.J. Kurzydlowski, D.W. Hutmacher, Repair and regeneration of osteochondral defects in the articular joints, Biomol. Eng. 24 (2007) 489–495, https://doi.org/10.1016/j.bioeng.2007.07.014.
[4] M. Navarro, A. Michiardi, O. Castano, J.A. Planell, Biomaterials in orthopaedics, 2008, https://doi.org/10.1098/rsif.2008.0151.
[5] J.M. Oliveira, S. Pina, R.L. Reis, J. San Roman (Eds.), Osteochondral Tissue Engineering: Challenges, Current Strategies, and Technological Advances, Springer International Publishing, Cham, 2018, https://doi.org/10.1007/978-3-319-76735-2.
[6] J.F. Mano, R.L. Reis, Osteochondral defects: present situation and tissue engineering approaches, J. Tissue Eng. Regen. Med. 1 (2007) 261–273, https://doi.org/10.1002/term.37.
[7] P. Gentile, I. Carmagnola, T. Nardo, V. Chiono, Layer-by-layer assembly for biomedical applications in the last decade, Nanotechnology 26 (2015), 422001, https://doi.org/10.1088/0957-4484/26/42/422001.
[8] G. Decher, J.D. Hong, J. Schmitt, Buildup of ultrathin multilayer films by a self-assembly process: III. Consecutively alternating adsorption of anionic and cationic polyelectrolytes on charged surfaces, Thin Solid Films 210–211 (1992) 831–835, https://doi.org/10.1016/0040-6090(92)90417-A.
[9] P. Gentile, I. Carmagnola, T. Nardo, V. Chiono, Layer-by-layer assembly for biomedical applications in the last decade, IOPscience (2015), https://doi.org/10.1088/0957-4484/26/42/422001.
[10] P. Gentile, M.E. Frongia, M. Cardellach, C.A. Miller, G.P. Stafford, G.J. Leggett, P. V. Hatton, Functionalised nanoscale coatings using layer-by-layer assembly for imparting antibacterial properties to polylactide-co-glycolide surfaces, Acta Biomater. 21 (2015) 35–43, https://doi.org/10.1016/j.actbio.2015.04.009.
[11] W. Li, T. Guan, X. Zhang, Z. Wang, M. Wang, W. Zhong, J. Kong, The Effect of Layer-by-Layer Assembly Coating on the Proliferation and Differentiation of Neural Stem Cells, ACS App. Mater. Interfaces (2015), https://doi.org/10.1021/am504456t.
[12] Y.T. Lai, E. Reading, G.L. Hura, K.L. Tsai, A. Laganowsky, F.J. Asturias, T.O. Yeates, Structure of a designed protein cage that self-assembles into a highly porous cube, Nat. Chem. (2014), https://doi.org/10.1038/nchem.2107.
[13] M. Zhao, G. Altankov, U. Grabiec, M. Bennett, M. Salmeron-Sanchez, F. Dehghani, T. Groth, Molecular composition of GAG-collagen I multilayers affects remodeling of terminal layers and osteogenic differentiation of adipose-derived stem cells, Acta Biomater. 41 (2016) 86–99, https://doi.org/10.1016/j.actbio.2016.05.023.
[14] H. Ai, S.A. Jones, Y.M. Lvov, Biomedical applications of electrostatic layer-by-layer nano-assembly of polymers 39 (2003) 23–44, https://doi.org/10.1385/CBB:39:1:23.
[15] D.P. Pioletti, O. Gauthier, V.A. Stadelmann, B. Bujoli, J. Guicheux, P.-Y. Zambelli, J.-M. Bouler, Orthopedic implant used as drug delivery system: clinical situation and state of the research, Curr. Drug Deliv. 5 (2008) 59–63, https://doi.org/10.2174/156720108783331041.
[16] B.S.G. Prasad, V.R.M. Gupta, N. Devanna, K. Jayasurya 5 (2014) 12.
[17] G. Khang, J.M. Rhee, J.K. Jeong, J.S. Lee, M.S. Kim, S.H. Cho, H.B. Lee, Local drug delivery system using biodegradable polymers, Macromol. Res. 11 (2003) 207–223, https://doi.org/10.1007/BF03218355.
[18] A. Aravamudhan, M.D. Ramos, J. Nip, A. Subramanian, R. James, D.M. Harmon, G. S. Kumbar, Osteoinductive small molecules: growth factor alternatives for bone tissue engineering, Curr. Pharm. Des. 19 (2013) 3420–3428, https://doi.org/10.2174/1381612811319190008.

[19] M. Yuasa, T. Yamada, T. Taniyama, T. Masaoka, W. Xuetao, T. Yoshii, S. Sotome, Dexamethasone Enhances Osteogenic Differentiation of Bone Marrow- and Muscle-Derived Stromal Cells and Augments Ectopic Bone Formation Induced by Bone Morphogenetic Protein-2, 2015, https://doi.org/10.1371/journal.pone.0116462.

[20] V. Llopis-Hernández, M. Cantini, C. González-García, Z.A. Cheng, J. Yang, P. M. Tsimbouri, A.J. García, M.J. Dalby, M. Salmerón-Sánchez, Material-driven fibronectin assembly for high-efficiency presentation of growth factors, Sci. Adv. 2 (2016), e1600188, https://doi.org/10.1126/sciadv.1600188.

[21] N. Monteiro, A. Martins, D. Ribeiro, S. Faria, N.A. Fonseca, J.N. Moreira, N. M. Neves, On the use of dexamethasone-loaded liposomes to induce the osteogenic differentiation of human mesenchymal stem cells, 2015, https://doi.org/10.1002/term.1817. Wiley Online Library.

[22] C. Wölk, C. Janich, U. Bakowsky, A. Langner, G. Brezesinski, Malonic acid based cationic lipids – the way to highly efficient DNA-carriers, Adv. Colloid Interf. Sci. 248 (2017) 20–34, https://doi.org/10.1016/j.cis.2017.08.003.

[23] S. Zhang, Y. Xu, B. Wang, W. Qiao, D. Liu, Z. Li, Cationic compounds used in lipoplexes and polyplexes for gene delivery, J. Control. Release 100 (2004) 165–180, https://doi.org/10.1016/j.jconrel.2004.08.019.

[24] J. Giselbrecht, C. Janich, S.R. Pinnapireddy, G. Hause, U. Bakowsky, C. Wölk, A. Langner, Overcoming the polycation dilemma – explorative studies to characterise the efficiency and biocompatibility of newly designed lipofection reagents, Int. J. Pharm. 541 (2018) 81–92, https://doi.org/10.1016/j.ijpharm.2018.02.029.

[25] X. Zhang, L. Dai, A. Wang, C. Wölk, B. Dobner, G. Brezesinski, J. Li, The directional observation of highly dynamic membrane tubule formation induced by engulfed liposomes, Sci. Rep. (2015), https://doi.org/10.1038/srep16559.

[26] C.R. Dass, P.F. Choong, Targeting of small molecule anticancer drugs to the tumour and its vasculature using cationic liposomes: lessons from gene therapy, SpringerLink, 2006, https://doi.org/10.1186/1475-2867-6-17.

[27] A. Kanazawa, T. Ikeda, T. Endo, Synthesis and antimicrobial activity of dimethyl- and trimethyl-substituted phosphonium salts with alkyl chains of various lengths, Antimicrob. Agents Chemother. (1994), https://doi.org/10.1128/AAC.38.5.945.

[28] C. Barnier Quer, A. Elsharkawy, S. Romeijn, A. Kros, W. Jiskoot, Cationic liposomes as adjuvants for influenza hemagglutinin: more than charge alone, Eur. J. Pharm. Biopharm. 81 (2012) 294–302, https://doi.org/10.1016/j.ejpb.2012.03.013.

[29] M.A. Mintzer, E. Simanek, E nonviral vectors for gene delivery, Chem. Rev. (2009), https://doi.org/10.1021/cr800409e.

[30] V.E. Santo, M.E. Gomes, J.F. Mano, R.L. Reis, Controlled release strategies for bone, cartilage, and osteochondral engineering—part I: recapitulation of native tissue healing and variables for the design of delivery systems, 2013, https://doi.org/10.1089/ten.teb.2012.0138.

[31] N. Patel 2 (2012) 7.

[32] M. Michel, D. Vautier, J.-C. Voegel, P. Schaaf, V. Ball, Layer by layer self-assembled polyelectrolyte multilayers with embedded phospholipid vesicles, Langmuir 20 (2004) 4835–4839, https://doi.org/10.1021/la049736q.

[33] D.V. Volodkin, P. Schaaf, H. Mohwald, J.-C. Voegel, V. Ball, Effective embedding of liposomes into polyelectrolyte multilayered films: the relative importance of lipid -polyelectrolyte and interpolyelectrolyte interactions, Soft Matter 5 (2009) 1394–1405, https://doi.org/10.1039/B815048F.

[34] N. Graf, A. Tanno, A. Dochter, N. Rothfuchs, J. Vörös, T. Zambelli, Electrochemically driven delivery to cells from vesicles embedded in polyelectrolyte multilayers, Soft Matter 8 (2012) 3641–3648, https://doi.org/10.1039/C2SM07272F.

[35] P.C. DeMuth, J.J. Moon, H. Suh, P.T. Hammond, D.J. Irvine, Releasable layer-by-layer assembly of stabilized lipid nanocapsules on microneedles for enhanced transcutaneous vaccine delivery, ACS Nano 6 (2012) 8041–8051, https://doi.org/10.1021/nn302639r.

[36] R. Polak, R.M. Lim, M.M. Beppu, R.N. Pitombo, R.E. Cohen, M.F. Rubner 4 (18) (2015) 2832–2841, https://doi.org/10.1002/adhm.201500604.

[37] V. Domínguez-Arca, R.R. Costa, A.M. Carvalho, P. Taboada, R.L. Reis, G. Prieto, I. Pashkuleva, Liposomes embedded in layer by layer constructs as simplistic extracellular vesicles transfer model, Mater. Sci. Eng. C 121 (2021), 111813, https://doi.org/10.1016/j.msec.2020.111813.

[38] X. Ma, X. Zhang, Y. Jia, S. Zu, S. Han, D. Xiao, H. Sun, Y. Wang, Dexamethasone induces osteogenesis via regulation of hedgehog signalling molecules in rat mesenchymal stem cells, Int. Orthop. 37 (2013) 1399–1404, https://doi.org/10.1007/s00264-013-1902-9.

[39] L. Zhao, G. Li, K.-M. Chan, Y. Wang, P.-F. Tang, Comparison of multipotent differentiation potentials of murine primary bone marrow stromal cells and mesenchymal stem cell line C3H10T1/2, Calcif. Tissue Int. 84 (2009) 56–64, https://doi.org/10.1007/s00223-008-9189-3.

[40] C.M. Shea, C.M. Edgar, T.A. Einhorn, L.C. Gerstenfeld, BMP treatment of C3H10T1/2 mesenchymal stem cells induces both chondrogenesis and osteogenesis, J. Cell. Biochem. 90 (2003) 1112–1127, https://doi.org/10.1002/jcb.10734.

[41] L. Han, A.J. Grodzinsky, C. Ortiz, Nanomechanics of the cartilage extracellular matrix, Annu. Rev. Mater. Res. 41 (2011) 133–168, https://doi.org/10.1146/annurev-matsci-062910-100431.

[42] F. Long, Building strong bones: molecular regulation of the osteoblast lineage, Nat. Rev. Mol. Cell Biol. (2012), https://doi.org/10.1038/nrm3254.

[43] O. Ghali, O. Broux, G. Falgayrac, N. Haren, J.P. van Leeuwen, G. Penel, P. Hardouin, C. Chauveau, Dexamethasone in osteogenic medium strongly induces adipocyte differentiation of mouse bone marrow stromal cells and increases osteoblast differentiation, BMC Cell Biol. 16 (2015), https://doi.org/10.1186/s12860-015-0056-6.

[44] F. Langenbach, J. Handschel, Effects of dexamethasone, ascorbic acid and β-glycerophosphate on the osteogenic differentiation of stem cells in vitro, Stem Cell Res Ther 4 (2013) 117, https://doi.org/10.1186/scrt328.

[45] I. Sekiya, P. Koopman, K. Tsuji, S. Mertin, V. Harley, Y. Yamada, K. Shinomiya, A. Nifuji, M. Noda, Dexamethasone enhances SOX9 expression in chondrocytes.

[46] Y.A. Brito Barrera, G. Hause, M. Menzel, C.E.H. Schmelzer, E. Lehner, K. Mäder, C. Wölk, T. Groth, Engineering osteogenic microenvironments by combination of multilayers from collagen type I and chondroitin sulfate with novel cationic liposomes, Mater. Today Bio. 7 (2020), 100071, https://doi.org/10.1016/j.mtbio.2020.100071.

[47] A. Köwitsch, M. Jurado Abreu, A. Chhalotre, M. Hielscher, S. Fischer, K. Mäder, T. Groth, Synthesis of thiolated glycosaminoglycans and grafting to solid surfaces, Carbohydr. Polym. 114 (2014) 344–351, https://doi.org/10.1016/j.carbpol.2014.08.027.

[48] U. Horzum, B. Ozdil, D. Pesen-Okvur, Step-by-step quantitative analysis of focal adhesions, MethodsX 1 (2014) 56–59, https://doi.org/10.1016/j.mex.2014.06.004.

[49] M. Sarem, O. Otto, S. Tanaka, V.P. Shastri, Cell number in mesenchymal stem cell aggregates dictates cell stiffness and chondrogenesis, Stem Cell Res. Ther. 10 (2019) 10, https://doi.org/10.1186/s13287-018-1103-y.

[50] K.J. Livak, T.D. Schmittgen, Analysis of relative gene expression data using real-time quantitative PCR and the $2-\Delta\Delta CT$ method, Methods 25 (2001) 402–408, https://doi.org/10.1006/meth.2001.1262.

[51] S. Tassler, B. Dobner, L. Lampp, R. Ziółkowski, E. Malinowska, C. Wölk, G. Brezesinski, DNA delivery systems based on peptide-mimicking cationic lipids—the effect of the co-lipid on the structure and DNA binding capacity, Langmuir 35 (2019) 4613–4625, https://doi.org/10.1021/acs.langmuir.8b04139.

[52] S. Tassler, C. Wölk, C. Janich, B. Dobner, G. Brezesinski, Lysine-based amino-functionalized lipids for gene transfection: the protonation state in monolayers at the air–liquid interface, Phys. Chem. Chem. Phys. 19 (2017) 20271–20280, https://doi.org/10.1039/C7CP03107F.

[53] J. Stetefeld, S.A. McKenna, T.R. Patel, Dynamic light scattering: a practical guide and applications in biomedical sciences, Biophys. Rev. 8 (2016) 409–427, https://doi.org/10.1007/s12551-016-0218-6.

[54] I.S. Zuhorn, U. Bakowsky, E. Polushkin, W.H. Visser, M.C.A. Stuart, J.B.F. N. Engberts, D. Hoekstra, Nonbilayer phase of lipoplex–membrane mixture determines endosomal escape of genetic cargo and transfection efficiency, Mol. Ther. 11 (2005) 801–810, https://doi.org/10.1016/j.ymthe.2004.12.018.

[55] M. Zhao, L. Li, C. Zhou, F. Heyroth, B. Fuhrmann, K. Maeder, T. Groth, Improved stability and cell response by intrinsic cross-linking of multilayers from collagen I and oxidized glycosaminoglycans, Biomacromolecules (2014), https://doi.org/10.1021/bm501286f.

[56] M. Zhao, R. Anouz, T. Groth, Effect of microenvironment on adhesion and differentiation of murine C3H10T1/2 cells cultured on multilayers containing collagen I and glycosaminoglycans, 2020, https://doi.org/10.1177/2041731420940560.

[57] C. Husteden, F. Doberenz, N. Goergen, S.R. Pinnapireddy, C. Janich, A. Langner, F. Syrowatka, A. Repanas, F. Erdmann, J. Jedelská, U. Bakowsky, T. Groth, C. Wölk, Contact-triggered lipofection from multilayer films designed as surfaces for in situ transfection strategies in tissue engineering, ACS Appl. Mater. Interfaces 12 (2020) 8963–8977, https://doi.org/10.1021/acsami.9b18968.

[58] P.D. Ward, S.L. Thibeault, S.D. Gray, Hyaluronic acid: its role in voice, J. Voice 16 (2002) 303–309, https://doi.org/10.1016/S0892-1997(02)00101-7.

[59] M. Michel, V. Toniazzo, D. Ruch, V. Ball, Deposition mechanisms in layer-by-layer or step-by-step deposition methods: from elastic and impermeable films to soft membranes with ion exchange properties, ISRN Mater. Sci. 2012 (2012), https://doi.org/10.5402/2012/701695.

[60] G. Altankov, K. Richau, T. Groth, The role of surface zeta potential and substratum chemistry for regulation of dermal fibroblasts interaction, in: Mater. Sci. Eng. Technol., Wiley Online Library, 2003, https://doi.org/10.1002/mawe.200300699.

[61] R. Zimmermann, O. Birkert, G. Gauglitz, C. Werner, Electrosurface Phenomena at Polymer Films for Biosensor Applications, 2003, https://doi.org/10.1002/cphc.200200475. Wiley Online Library.

[62] J. Almodóvar, L.W. Place, J. Gogolski, K. Erickson, M.J. Kipper, layer-by-layer assembly of polysaccharide-based polyelectrolyte multilayers: a spectroscopic study of hydrophilicity, composition, and ion pairing, Biomacromolecules 12 (2011) 2755–2765, https://doi.org/10.1021/bm200519y.

[63] M.S. Niepel, K. Kirchhof, M. Menzel, A. Heilmann, T. Groth, Controlling cell adhesion using ph-modified polyelectrolyte multilayer films, in: Layer-by-layer Films for Biomedical Applications, John Wiley & Sons, Ltd, 2015, pp. 1–30, https://doi.org/10.1002/9783527675869.ch1.

[64] G. Altankov, F. Grinnell, T. Groth, Studies on the biocompatibility of materials: Fibroblast reorganization of substratum-bound fibronectin on surfaces varying in wettability, 1996, https://doi.org/10.1002/(SICI)1097-4636(199603)30:3<385::AID-JBM13>3.0.CO;2-J. Wiley Online Library.

[65] N. Faucheux, R. Schweiss, K. Lützow, C. Werner, T. Groth, Self-assembled monolayers with different terminating groups as model substrates for cell adhesion studies, Biomaterials 25 (2004) 2721–2730, https://doi.org/10.1016/j.biomaterials.2003.09.069.

[66] M. Schönhoff, Layered polyelectrolyte complexes: physics of formation and molecular properties, J. Phys. Condens. Matter 15 (2003) R1781–R1808, https://doi.org/10.1088/0953-8984/15/49/R01.

[67] R. McBeath, D.M. Pirone, C.M. Nelson, K. Bhadriraju, C.S. Chen, Cell shape, cytoskeletal tension, and RhoA regulate stem cell lineage commitment, Dev. Cell 6 (2004) 483–495, https://doi.org/10.1016/S1534-5807(04)00075-9.

[68] W.H. Goldmann, Role of vinculin in cellular mechanotransduction, 2016, https://doi.org/10.1002/cbin.10563. Wiley Online Library.
[69] M. Bennett, M. Cantini, J. Reboud, J.M. Cooper, P. Roca-Cusachs, M. Salmeron-Sanchez, Molecular clutch drives cell response to surface viscosity, PNAS 115 (2018) 1192–1197, https://doi.org/10.1073/pnas.1710653115.
[70] D.E. Discher, P. Janmey, Y. Wang, Tissue cells feel and respond to the stiffness of their substrate, Science 310 (2005) 1139–1143, https://doi.org/10.1126/science.1116995.
[71] A.S. Mao, J.-W. Shin, D.J. Mooney, Effects of substrate stiffness and cell-cell contact on mesenchymal stem cell differentiation, Biomaterials 98 (2016) 184–191, https://doi.org/10.1016/j.biomaterials.2016.05.004.
[72] A. Nolte, S. Hossfeld, B. Schroeppel, A. Mueller, D. Stoll, T. Walker, R. Krastev, Impact of polyelectrolytes and their corresponding multilayers to human primary endothelial cells, J. Biomater. Appl. (2013), https://doi.org/10.1177/0885328212437610.
[73] V. Gribova, R. Auzely-Velty, C. Picart, Polyelectrolyte multilayer assemblies on materials surfaces: from cell adhesion to tissue engineering, Chem. Mater. (2013), https://doi.org/10.1021/cm2032459.
[74] T. Groth, Z.M. Liu, M. Niepel, D. Peschel, K. Kirchhof, G. Altankov, N. Faucheux, Chemical and Physical Modifications of Biomaterial Surfaces to Control Adhesion of Cells, SpringerLink, 2010, https://doi.org/10.1007/978-90-481-8790-4_13.
[75] M. Kisiel, M.M. Martino, M. Ventura, J.A. Hubbell, J. Hilborn, D.A. Ossipov, Improving the osteogenic potential of BMP-2 with hyaluronic acid hydrogel modified with integrin-specific fibronectin fragment, Biomaterials 34 (2013) 704–712, https://doi.org/10.1016/j.biomaterials.2012.10.015.
[76] H. Ponta, L. Sherman, P.A. Herrlich, CD44: from adhesion molecules to signalling regulators, Nat. Rev. Mol. Cell. Biol. 4 (2003) 33–45, https://doi.org/10.1038/nrm1004.
[77] J. Jokinen, E. Dadu, P. Nykvist, J. Käpylä, D.J. White, J. Ivaska, P. Vehviläinen, H. Reunanen, H. Larjava, L. Häkkinen, J. Heino, Integrin-mediated cell adhesion to type I collagen fibrils, J. Biol. Chem. 279 (2004) 31956–31963, https://doi.org/10.1074/jbc.M401409200. *.
[78] P.J. Wrighton, J.R. Klim, B.A. Hernandez, C.H. Koonce, T.J. Kamp, L.L. Kiessling, Signals from the surface modulate differentiation of human pluripotent stem cells through glycosaminoglycans and integrins, 2014, https://doi.org/10.1073/pnas.1409525111.
[79] J.D. Humphrey, E.R. Dufresne, M.A. Schwartz, Mechanotransduction and extracellular matrix homeostasis, Nat. Rev. Mol. Cell. Biol. 15 (2014) 802–812, https://doi.org/10.1038/nrm3896.
[80] A.J. García, Get a grip: integrins in cell–biomaterial interactions, ScienceDirect (2005), https://doi.org/10.1016/j.biomaterials.2005.05.029.
[81] X. Wu, S. Ding, Q. Ding, N.S. Gray, P.G. Schultz, A small molecule with osteogenesis-inducing activity in multipotent mesenchymal progenitor cells, J. Am. Chem. Soc. 124 (2002) 14520–14521, https://doi.org/10.1021/ja0283908.
[82] K.M. Sinha, X. Zhou, Genetic and molecular control of osterix in skeletal formation, J. Cell. Biochem. 114 (2013) 975–984, https://doi.org/10.1002/jcb.24439.
[83] A. Cheng, P.G. Genever, SOX9 determines RUNX2 transactivity by directing intracellular degradation 25 (2010) 2680–2689, https://doi.org/10.1002/jbmr.174.
[84] F. Jafary, P. Hanachi, K. Gorjipour, Osteoblast differentiation on collagen scaffold with immobilized alkaline phosphatase, Int. J. Organ Transplant Med. 8 (2017) 195–202.
[85] J. Settleman, Tension precedes commitment—even for a stem cell, Mol. Cell 14 (2004) 148–150, https://doi.org/10.1016/S1097-2765(04)00207-2.
[86] I. Sekiya, P. Koopman, K. Tsuji, S. Mertin, V. Harley, Y. Yamada, K. Shinomiya, A. Nifuji, M. Noda, Dexamethasone enhances SOX9 expression in chondrocytes, J. Endocrinol. 169 (2001) 573–579, https://doi.org/10.1677/joe.0.1690573.
[87] M.A. Pratta, W. Yao, C. Decicco, M.D. Tortorella, R.-Q. Liu, R.A. Copeland, R. Magolda, R.C. Newton, J.M. Trzaskos, E.C. Arner, Aggrecan protects cartilage collagen from proteolytic cleavage, J. Biol. Chem. 278 (2003) 45539–45545, https://doi.org/10.1074/jbc.M303737200.
[88] H. Tanaka, C.L. Murphy, C. Murphy, M. Kimura, S. Kawai, J.M. Polak, Chondrogenic differentiation of murine embryonic stem cells: effects of culture conditions and dexamethasone, J. Cell. Biochem. 93 (2004) 454–462, https://doi.org/10.1002/jcb.20171.
[89] A.C. Daly, S.E. Critchley, E.M. Rencsok, D.J. Kelly, A comparison of different bioinks for 3D bioprinting of fibrocartilage and hyaline cartilage, Biofabrication 8 (2016), 045002, https://doi.org/10.1088/1758-5090/8/4/045002.
[90] M.K. Gordon, R.A. Hahn, Collagens, Cell Tissue Res. 339 (1) (2010) 247–257, https://doi.org/10.1007/s00441-009-0844-4.
[91] M.S. Niepel, B.K. Ekambaram, C.E.H. Schmelzer, T. Groth, Polyelectrolyte multilayers of poly (l-lysine) and hyaluronic acid on nanostructured surfaces affect stem cell response, Nanoscale 11 (2019) 2878–2891, https://doi.org/10.1039/c8nr05529g.
[92] L. Yang, K.Y. Tsang, H.C. Tang, D. Chan, K.S.E. Cheah, Hypertrophic chondrocytes can become osteoblasts and osteocytes in endochondral bone formation, PNAS 111 (2014) 12097–12102, https://doi.org/10.1073/pnas.1302703111.
[93] L. Gao, R. McBeath, C.S. Chen, Stem cell shape regulates a chondrogenic versus myogenic fate through Rac1 and N-cadherin, Stem Cells 28 (3) (2010) 564–572, https://doi.org/10.1002/steam.308.